


Review

Astroparticle Physics with Compact Objects

Peter Tinyakov ¹ , Maxim Pshirkov ^{2,3,4}  and Sergei Popov ^{2,*} 

¹ Service de Physique Theorique, Université Libre de Bruxelles, Service de Physique Théorique, Boulevard du Triomphe, CP225, 1050 Brussels, Belgium; petr.tiniakov@ulb.be

² Sternberg Astronomical Institute, Lomonosov Moscow State University, 119234 Moscow, Russia; pshirkov@gmail.com

³ Institute for Nuclear Research of Russian Academy of Sciences, 60th October Anniversary Prospect, 7a, 117312 Moscow, Russia

⁴ P. N. Lebedev Physical Institute of the Russian Academy of Sciences, Pushchino Radio Astronomy Observatory (PRAO), 142290 Pushchino, Russia

* Correspondence: sergепolar@gmail.com; Tel.: +7-495-939-5006

Abstract: Probing the existence of hypothetical particles beyond the Standard model often deals with extreme parameters: large energies, tiny cross-sections, large time scales, etc. Sometimes, laboratory experiments can test required regions of parameter space, but more often natural limitations lead to poorly restrictive upper limits. In such cases, astrophysical studies can help to expand the range of values significantly. Among astronomical sources, used in interests of fundamental physics, compact objects—neutron stars and white dwarfs—play a leading role. We review several aspects of astroparticle physics studies related to observations and properties of these celestial bodies. Dark matter particles can be collected inside compact objects resulting in additional heating or collapse. We summarize regimes and rates of particle capturing as well as possible astrophysical consequences. Then, we focus on a particular type of hypothetical particles—axions. Their existence can be uncovered due to observations of emission originated due to the Primakoff process in magnetospheres of neutron stars or white dwarfs. Alternatively, they can contribute to the cooling of these compact objects. We present results in these areas, including upper limits based on recent observations.

Keywords: dark matter; axions; neutron stars; white dwarfs



Citation: Tinyakov, P.; Pshirkov, M.; Popov, S. Astroparticle Physics with Compact Objects. *Universe* **2021**, *7*, 401. <https://doi.org/10.3390/universe7110401>

Academic Editor: Daniela D. Doneva

Received: 28 September 2021

Accepted: 18 October 2021

Published: 25 October 2021

Publisher's Note: MDPI stays neutral with regard to jurisdictional claims in published maps and institutional affiliations.



Copyright: © 2021 by the authors. Licensee MDPI, Basel, Switzerland. This article is an open access article distributed under the terms and conditions of the Creative Commons Attribution (CC BY) license (<https://creativecommons.org/licenses/by/4.0/>).

1. Introduction

It is a commonplace to state that compact objects—white dwarfs, neutron stars, and black holes—are unique natural laboratories which allow us to study matter and various processes under extreme conditions. However, this is indeed true and quite often best limits on different hypotheses in fundamental physics beyond standard scenarios are given by observations of these astrophysical sources.

Leaving black holes (BHs) aside, neutron stars (NSs) and white dwarfs (WDs) with their high density and temperature of interiors and large external and internal magnetic fields in many respects are well-suited for studies of interactions with even very elusive particles (like dark matter candidates, axions and axion-like particles, etc.) and for their production.

Internal densities of NSs can reach up to $\lesssim 10$ nuclear saturation density [1]. This allows for obtaining a reasonable rate of interaction even with particles with a very small cross-section reducing their energy in the process and eventually trapping them inside compact objects. Despite WDs having about seven orders of magnitude lower density, they also can capture weakly interacting particles.

High densities combined with high temperatures result in non-trivial cooling processes of compact objects which are born very hot. The main cooling channel for many of them is related to neutrino emission [2]. However, it was also proposed that axions can play a role in thermal energy losses in both NSs and WDs (see, e.g., [3,4]).

In the case of magnetars [5] and magnetic WDs (MWDs) [6], magnetic moments can be as high as 10^{33} G cm³. Magnetospheres of such compact objects can interact with axions via the Primakoff process, thus working as a kind of a haloscope [7]. Typically, magnetic fields of other astronomical objects (or in realistic medium) are not that high to produce a significant effect for discussed parameters of particles. Thus, NSs and WDs can give us a unique opportunity to discover axions with purely astrophysical methods.

In this review, BHs generally are not discussed, together with different exotic solutions like boson stars [8], fermion stars [9], pion stars [10], etc. Instead we focus on three above-mentioned aspects linking particle physics beyond the Standard model with properties of NSs and WDs.

At first, in Section 2, we discuss how dark matter (DM) particles can appear inside NSs and WDs due to capturing by progenitors or already after the compact object formation. Then, studies of the main possible consequences—heating and collapse—of particles capture are reviewed.

In the next section, we turn to a specific type of hypothetical particles—axions (including so-called axion-like particles, ALPs). We present a theory of axion interaction with magnetospheres of NSs. We discuss interactions with axions of cosmological origin that could constitute dark matter and those produced in NSs. Interaction of axion clusters with magnetospheres is also discussed in the context of models of fast radio bursts (FRBs) origin.

Finally, in Section 4, we come to WDs and review the possible role of axions in the cooling of these compact objects; after which, they present several upper limits on properties of these particles based on observations of WDs.

2. Compact Objects and Dark Matter

According to the theory of structure formation, at galactic and larger scales, the distributions of baryons and dark matter are correlated. Stars are therefore formed in regions of DM overdensities. As any gravitating objects, they have some amount of DM gravitationally bound to them. They may also accumulate DM during their lifetime. While the total amount of the accumulated DM stays tiny, it may nevertheless have observable effects. In this section, we review the DM capture mechanisms and estimate the amount of DM that may be accumulated by a star in different conditions. We then discuss possible observational signatures that may result.

2.1. Capture of DM By Stars

Stars capture DM at formation and during their lifetime by two different mechanisms. The second one—accumulation during the star lifetime—requires non-zero DM-to-nucleon interactions for capture; the first mechanism is gravitational at the stage of capture but still requires DM interactions with nucleons for the thermalization of the captured DM. The two mechanisms generally give comparable contributions to the total amount of DM accumulated by a star. We start with the second one as it is more extensively studied in the literature and allows for simple analytical estimates.

2.1.1. Capture during Star Lifetime

To gain a qualitative understanding of the capture mechanism, consider an isolated star (an enhancement of capture rate may be expected in binary systems, but only by a factor of a few [11]), embedded in a gas of non-interacting DM particles, as would be the case for stars in galactic halos. Assume the DM distribution in velocities is Maxwellian, characterized by a velocity dispersion \bar{v} . Assume as well that the star is at rest with respect to the DM distribution. This is not the case for most of the stars in halos as their typical velocities are the same as those of DM particles that is of order \bar{v} . In addition, the DM distribution in velocities may not be Gaussian in a realistic halo. We will discuss later the effect of these complications on the capture rate.

The star forms a gravitational potential well where DM particles are confined provided they have negative total energy. A particle from the DM halo that originally has a positive

energy can lose it in collisions with the stellar material and become gravitationally bound. Since the collisions happen while a particle is inside the star, it settles on a star-crossing orbit and will eventually come back and cross the star again. The energy losses will thus continue until the particle reaches an equilibrium with the matter inside the star. The rate of capture is determined by the number of particles that get gravitationally bound after the first star crossing.

It follows immediately from this picture that there is an upper bound on the capture rate F independent of the energy loss mechanism. It is given by the rate of star crossings by the DM particles. For a given particle with asymptotic velocity, v , the cross section of the star crossing is

$$\sigma_{\text{cross}} = \pi R_*^2 \left(1 + \frac{2GM_*}{R_* v^2} \right) = \pi R_*^2 \left(1 + \frac{v_{\text{esc}}^2}{v^2} \right), \tag{1}$$

where R_* and M_* are the star radius and mass, G is the gravitational constant, and v_{esc} the escape velocity from the surface of the star. Here, for simplicity, the Newtonian gravity has been assumed, which gives a reasonable approximation even for a NS. The account for General Relativity corrections changes the capture rate by a factor of order 1 [12]. The second term in the parenthesis is the result of gravitational focusing; this term is dominant in most cases. Averaging this expression over the Maxwellian distribution of the velocity dispersion \bar{v} yields the maximum value of the DM capture rate F ,

$$F_{\text{max}} = \left(\frac{8\pi}{3} \right)^{1/2} n R_*^2 \bar{v} \left(1 + \frac{3v_{\text{esc}}^2}{2\bar{v}^2} \right) \simeq \sqrt{6\pi} n R_*^2 v_{\text{esc}}^2 / \bar{v} = \sqrt{6\pi} n \frac{R_* R_g c^2}{\bar{v}}, \tag{2}$$

where n is the DM number density and $R_g = 2GM_*/c^2$ is a stellar gravitational radius. In the final expression, we have neglected the first term in the r.h.s. of Equation (1) as compared to the second one. Detailed calculations can be found in Refs. [13–15]. Equation (2) suggests that loosely bound haloes with smaller velocity dispersion give higher capture rates.

To get an idea of how much DM can possibly be captured by this mechanism, let us substitute the numbers. For a Sun-like star in the typical Galactic environment, assuming the lifetime of 10 Gyr Equation (2) gives for the total mass of the accumulated DM $M_{\text{tot}} \sim 5 \times 10^{47} \text{ GeV} \sim 5 \times 10^{-10} M_{\odot}$. For an NS in the same conditions, $M_{\text{tot}} \sim 10^{43} \text{ GeV} \sim 10^{-14} M_{\odot}$. The upper limits may be higher by 2–3 orders of magnitude in an environment with higher DM density and smaller velocity.

The capture rate, however, is usually further suppressed for two reasons: not every particle that crosses the star may get scattered, and, even if it does, not every particle loses enough energy to become gravitationally bound. The scattering is controlled by the cross section of DM interactions with nucleons. There is a critical value of this cross section σ_{cr} at which the star becomes opaque to DM particles, that is, at which a DM particle scatters once per crossing on average. It is estimated as $\sigma_{\text{cr}} = R_*^2 m_p / M_*$ and has the following value for the Sun, a WD and a NS, respectively:

$$\begin{aligned} \sigma_{\text{cr, Sun}} &\simeq 4 \times 10^{-36} \text{ cm}^2, \\ \sigma_{\text{cr, WD}} &\simeq 4 \times 10^{-40} \text{ cm}^2, \\ \sigma_{\text{cr, NS}} &\simeq 8 \times 10^{-46} \text{ cm}^2. \end{aligned} \tag{3}$$

For NSs and WDs, we have neglected the effects of matter degeneracy; they will be commented on later. If the DM-nucleon cross section is smaller than the critical one, the capture rate gets proportionally suppressed. Note that this is a likely case as the experimental bounds on the DM-nucleon cross section $\sigma_{\text{DM-n}}$ are becoming quite strict. In the case of the spin-independent interactions, they are at the level of 10^{-46} cm^2 at DM mass around 50 GeV [16], while for the spin-dependent interactions the limits on the cross

section are at the level of $10^{-40} - 10^{-41} \text{ cm}^2$ [17–20]. The constraints become much weaker for DM masses below 10 GeV and higher than several TeV.

Consider now the effect of energy losses on the capture rate. A particle crossing the star gets trapped if it loses the energy E_{loss} which is larger than its asymptotic energy. If $E_{\text{loss}} \gtrsim m\bar{v}^2/2$, most of the particles crossing the star get trapped and no additional suppression results as compared to Equation (2). In the opposite case, only a fraction of particles that have sufficiently small asymptotic velocity $v < \bar{v}$ such that $mv^2/2 < E_{\text{loss}}$ will become gravitationally bound. Given that the distribution of DM particles over velocities, it is a matter of a direct calculation to find the capture as a function of E_{loss} . Assuming all particles lose the same energy, one gets the capture rate

$$F = \sqrt{6\pi} \frac{\rho_{\text{DM}} R_* R_g}{m\bar{v}(1 - R_g/R_*)} \left[1 - \exp\left(-\frac{3E_{\text{loss}}}{m\bar{v}^2}\right) \right] f. \tag{4}$$

Here, ρ_{DM} is the DM ambient density, and f is the fraction of particles that scatter among all particles crossing the star

$$\begin{aligned} f &= \sigma/\sigma_{\text{cr}} && \text{if } \sigma < \sigma_{\text{cr}}, \\ f &= 1 && \text{otherwise.} \end{aligned} \tag{5}$$

For completeness, we have also included in Equation (4) the relativistic correction $1/(1 - R_g/R_*)$ [12], which, however, is only noticeable in case of NSs, where it leads to a slight enhancement of the rate. We will disregard it in what follows.

The dependence of the capture rate on the energy loss E_{loss} is controlled by the factor in the square brackets. When the energy loss in a single star crossing is of an order larger than the typical asymptotic energy $m\bar{v}^2/2$, this factor is close to 1 and gives no extra suppression of the capture rate. In this case, and, assuming all particles scatter ($f = 1$), one recovers the maximum rate (2). Note that, in this regime, the mass capture rate mF is independent of the DM mass m at a given ambient DM density ρ_{DM} . In the opposite limit when the energy losses are small, $E_{\text{loss}} \ll m\bar{v}^2$, the capture rate is further suppressed. In this regime, the mass capture rate is inversely proportional to the DM mass. Note also that in this case the dependence on the DM asymptotic velocity is much stronger, $F \propto 1/\bar{v}^3$. In summary,

$$F \simeq \begin{cases} \sqrt{6\pi} \frac{\rho_{\text{DM}} R_* R_g}{m\bar{v}} f & \text{at large } E_{\text{loss}} \gg m\bar{v}^2, \\ \sqrt{6\pi} \frac{\rho_{\text{DM}} R_* R_g}{m\bar{v}} \frac{3E_{\text{loss}}}{m\bar{v}^2} f & \text{at small } E_{\text{loss}} \ll m\bar{v}^2. \end{cases} \tag{6}$$

The extra suppression factor $\propto E_{\text{loss}}/(m\bar{v}^2)$ at small E_{loss} arises because, in this case, only a small fraction of the DM particles—those that have $mv^2 \lesssim E_{\text{loss}}$ —can lose enough energy in one star crossing and become gravitationally bound. Clearly, in this regime, only the low-velocity part of the DM distribution is important. The velocity dependence of the capture rate (6) originates in this case from the volume element in the velocity space d^3v and will be the same for any velocity distribution that, like the Maxwellian one, goes to a constant at small v . Therefore, regardless of the details of the DM velocity distribution, the capture rate is proportional to $F \propto 1/\bar{v}$ and is given by Equation (2) times the probability of scattering f for small \bar{v} , and changes to $F \propto 1/\bar{v}^3$ as given by the small E_{loss} case of Equation (6) with possibly a different numerical coefficient.

When expressed in terms of the energy loss E_{loss} and the probability of scattering f , Equation (6) is completely general and applies to any type of DM and/or stars. The specific features of the models determine these two quantities. The probability f is determined by the scattering cross section through Equation (5) for particle DM, for primordial black holes $f = 1$.

Consider now the energy losses E_{loss} . We start with the simplest case of particle DM crossing an ordinary star. A typical kinetic energy of a DM particle away from the star is $m\bar{v}^2/2$. When the particle falls onto the star, it accelerates and picks the velocity of order of the escape velocity. For a Sun-like star, the latter is ~ 600 km/s, which is about factor 3 higher than the dispersion velocity in our Galaxy at the position of the Sun. We can therefore estimate the particle velocity while crossing the star as the escape velocity $v_{\text{esc}} \propto \sqrt{R_g/R_*}$. At the temperature of order 10^7 K, the protons in the core of a Sun-like star move with the thermal velocity $\sqrt{3kT/m_p} \sim 500$ km/s, and with smaller velocities away from the core. For the sake of the estimate, we may, therefore, consider the collision of DM particles with protons at rest. Assume, for simplicity, that DM particles are much heavier than protons. The typical energy transfer in the collision, in the frame of the star, is then $E_{\text{loss}} \sim m_p v_{\text{rel}}^2/2$, where $v_{\text{rel}} \sim v_{\text{esc}}$ is the relative velocity of particles. Depending on the environment, this energy loss may be larger or smaller than the particle asymptotic energy. In our Galaxy and for DM particles heavier than ~ 10 GeV, the energy loss is smaller than typical asymptotic energy, so we are in the suppressed small E_{loss} regime of Equation (6). In dwarf galaxies with typical velocity dispersion ~ 10 km/s, this regime occurs for DM masses $\gtrsim 500$ GeV; otherwise, the large E_{loss} regime of Equation (6) gives the right estimate of the rate. Thus, in these two cases, we have for the mass capture rate:

Sun-like, Milky Way:

$$mF \sim 2 \times 10^{30} \text{ GeV/s} \left(\frac{\rho_{\text{DM}}}{0.5 \text{ GeV/cm}^3} \right) \left(\frac{10 \text{ GeV}}{m} \right) f, \tag{7}$$

Sun-like, dwarf galaxies, $m \gtrsim 500$ GeV:

$$mF \sim 9 \times 10^{34} \text{ GeV/s} \left(\frac{\rho_{\text{DM}}}{100 \text{ GeV/cm}^3} \right) \left(\frac{500 \text{ GeV}}{m} \right) f, \tag{8}$$

Sun-like, dwarf galaxies, $m \lesssim 500$ GeV:

$$mF \sim 9 \times 10^{34} \text{ GeV/s} \left(\frac{\rho_{\text{DM}}}{100 \text{ GeV/cm}^3} \right) f, \tag{9}$$

The numerical values in Equations (7)–(9) are close to the maximum achievable capture rates for the Sun-like star in the corresponding environment. Note, however, that, in view of Equation (3), (5) for the Sun-like star the scattering probability is $f \lesssim 10^{-10}$ if current experimental bounds on the spin-independent DM-nucleon cross section are assumed.

In the case of compact objects—WDs or NSs—the escape velocities are substantially higher, $v_{\text{esc}} \sim 6 \times 10^3$ km/s and $v_{\text{esc}} \sim 0.5c$, respectively. In this case, we are always in the large E_{loss} regime of Equation (6) for DM masses below ~ 1 TeV. The capture rate is then estimated as follows:

$$\text{WD: } mF \sim 2 \times 10^{28} \text{ GeV/s} \left(\frac{\rho_{\text{DM}}}{0.5 \text{ GeV/cm}^3} \right) \left(\frac{220 \text{ km/s}}{\bar{v}} \right) f, \tag{10}$$

$$\text{NS: } mF \sim 2.5 \times 10^{26} \text{ GeV/s} \left(\frac{\rho_{\text{DM}}}{0.5 \text{ GeV/cm}^3} \right) \left(\frac{220 \text{ km/s}}{\bar{v}} \right) f. \tag{11}$$

In the case of compact stars, the critical cross sections are smaller, cf. Equation (3), so the scattering probability f is less suppressed than in the case of Sun-like stars. For NSs, assuming current experimental limits on the scattering cross section, it may reach values close to 1 even for the spin-independent cross section. In all cases, however, the accumulation rates are small: only a tiny fraction of M_{\odot} can be accumulated over the age of the Universe.

A number of subtleties arises in the case of capture by NSs because NS matter is degenerate, and because the scattering happens at semi-relativistic velocities. A detailed analysis of these subtleties and further discussion can be found in Ref. [21–23]. Note that

the estimates presented above neglect the self-interactions of DM particles. Accounting for such self-interactions may in some cases significantly change (enhances) the capture rate [24].

2.1.2. Capture at Star Formation

In addition to the DM accumulated during the lifetime, stars capture some amount of DM in the process of their formation. This capture mechanism is different from the accumulation considered in the previous section as its first stage is gravitational and thus is independent of the DM properties. We summarise here this mechanism following Refs. [25,26].

Stars are formed from the pre-stellar cores. These baryonic overdensities create dips in the gravitational potential filled with slow DM particles bound to the pre-stellar core. These slow particles are, of course, only a small fraction of the ambient DM density, and their mass density is completely negligible to that of the baryons. When the star forms, this bound DM is dragged along by the time-dependent gravitational field of contracting baryons. This process is slow in the sense that the star formation time, being determined by the energy dissipation by the baryons, is much larger than the free fall time. It can therefore be described in the adiabatic approximation. When the star is finally formed, the space distribution of the bound DM becomes peaked at the star position. This is the first stage of the DM capture.

Among the DM particles that form the resulting cuspy profile of interest to us are those that have trajectories crossing the newly-born star. These particles are in the same conditions as the ones captured by direct scattering (cf. Section 2.1.1): they will sooner or later scatter off the star nucleons, lose their energy, and settle inside the star.

The amount of DM that is captured in this way is proportional to the density of DM that was gravitationally bound to the pre-stellar core, and depends on the parameters of the DM distribution after the adiabatic contraction of baryons. The bound DM density can be estimated in terms of the depth of the gravitational potential of the pre-stellar core ϕ as follows:

$$\rho_{\text{bound}} = \rho_{\text{DM}} \frac{4\pi}{3} \left(\frac{3\phi}{\pi\bar{v}^2} \right)^{3/2}, \quad (12)$$

where ρ_{DM} is the ambient DM density and its velocity distribution is assumed to be Gaussian with the characteristic velocity \bar{v} . The gravitational potential in turn can be estimated in terms of the parameters of the pre-stellar core and is in the range 3×10^{-12} – 3×10^{-11} for stellar masses $1 - 10 M_{\odot}$ [25]. In all cases, one has $\rho_{\text{bound}}/\rho_{\text{DM}} \ll 1$.

The distribution of the bound DM after the contraction of baryons can be calculated numerically. The simulation is straightforward due to two simplifications: the contribution of the DM into the gravitational potential is negligible, and therefore particle trajectories may be simulated one at a time, and the process is adiabatic so that the details of the baryonic contraction are irrelevant as long as it is sufficiently slow (in practice, several times slower than the free fall time is enough). Combining the results of Refs. [25,26], one obtains the following estimates of the total mass of the DM that acquires orbits crossing the star and may eventually be captured, for two different star masses:

$$M_{\odot}: \quad M_{\text{tot}} \sim 2 \times 10^{-13} M_{\odot} \left(\frac{\rho_{\text{DM}}}{100 \text{ GeV/cm}^3} \right) \left(\frac{10 \text{ km/s}}{\bar{v}} \right)^3, \quad (13)$$

$$10 M_{\odot}: \quad M_{\text{tot}} \sim 6 \times 10^{-11} M_{\odot} \left(\frac{\rho_{\text{DM}}}{100 \text{ GeV/cm}^3} \right) \left(\frac{10 \text{ km/s}}{\bar{v}} \right)^3. \quad (14)$$

These numbers can be compared to Equation (9). Taking $f \sim 10^{-10}$ and assuming for a Sun-like star lifetime ~ 10 Gyr one has from direct capture, Equation (9), $M_{\text{tot}} \sim 3 \times 10^{-15} M_{\odot}$ for the same environment of a typical dwarf galaxy. We see that capture

at the stage of star formation may give a dominant contribution to the total amount of accumulated DM.

2.1.3. Thermalization of Captured DM

Both mechanisms that have been described above require that DM particles which have been captured on bound star-crossing orbits interact with the stellar nucleons in order to eventually settle inside the star. This thermalization process takes time that is controlled by the DM parameters: the mass m and the cross section σ of DM with nucleons. The thermalization time can be estimated as follows [27]. One has to consider separately two stages. At the first stage, the DM trajectories are mostly outside of the star while crossing it twice per period. At the second stage, the DM particles move on orbits completely contained inside the star. In both cases, the energy loss happens over many orbits and can be described by a differential equation in a continuous energy loss approximation. Solving this differential equation gives the thermalization times for the two stages. For the second stage, the initial conditions are the same for both capture mechanisms considered previously, and one has

$$t_2 = \frac{m^{3/2}}{\sqrt{3\rho_*\sigma}} \frac{1}{\sqrt{kT_*}} \sim 64\text{yr} \left(\frac{m}{100\text{ GeV}}\right)^{3/2} \left(\frac{10^{-36}\text{ cm}^2}{\sigma}\right), \tag{15}$$

where T_* is the star core temperature which determines the final particle energy.

For the first stage, the initial conditions are different for the two capture mechanisms. In the case of direct capture, they are set by the energy loss in the first collision. One has [27]:

$$t_1 \sim \frac{3\pi m R_*^{3/2} \sigma_{\text{cr}}}{4m_p R_g^{1/2} \sigma} \sqrt{\left|\frac{E_*}{E_0}\right|} \sim 20\text{yr} \left(\frac{m}{100\text{ GeV}}\right)^{3/2} \left(\frac{10^{-36}\text{ cm}^2}{\sigma}\right), \tag{16}$$

where R_* is the stellar radius, R_g is its gravitational radius, m_p is proton mass, $E_* = GMm/R_*$ is the particle binding energy at the star surface, and $E_0 = m_p c^2 R_g/R_*$ is a typical energy loss in the first collision, so that $E_*/E_0 \sim m/m_p$. In the case of the direct capture by a NS the parameters of the NS should be used in these estimates. Assuming $\sigma \sim \sigma_{\text{cr}}$, Equations (15) and (16) then give $t_1 \sim 0.16\text{ s}$, $t_2 \sim 100\text{ s}$ for $m = 100\text{ GeV}$, i.e., in this case the thermalization time is negligibly short.

For the capture at formation, the initial conditions are determined by the size of the pre-stellar core which sets the size of largest orbits. The ratio of the final to initial energy becomes instead $E_*/E_0 \sim R_{\text{psc}}/R_*$ where R_{psc} is the radius of the pre-stellar core. At $m = 100\text{ GeV}$, this gives an extra factor 100 in the thermalization time, so that

$$t_1 \sim 2 \times 10^3\text{ yr} \left(\frac{m}{100\text{ GeV}}\right) \left(\frac{10^{-36}\text{ cm}^2}{\sigma}\right). \tag{17}$$

The thermalization time becomes much larger than the age of the Universe for allowed spin-independent cross sections and DM masses in the 100 GeV range.

The above estimates of the thermalization time have to be modified in the case of a direct capture by the NS. In this case, the degeneracy of the nuclear matter has to be taken into account. For heavy DM, the modifications are not dramatic [27,28] because, in the case of a neutron star, DM particles falling onto the star have semi-relativistic velocities, so that, for particles much heavier than protons, the momentum transfer is of the order of the neutron Fermi momentum. For lighter DM particles, the modifications are large. The recent detailed calculations can be found in Refs. [29–32]. In case of very small interaction cross-sections, $\sigma \ll 10^{-36}\text{ cm}^2$, and corresponding long thermalization times, the capture process could be affected by the influence of external perturbers, which would prevent some particles from moving into completely contained orbits [33].

Once the DM particles thermalize with the star, they form a spherical cloud in the center of a radius

$$r_{\text{th}} = \left(\frac{9T_*}{8\pi G\rho_* m} \right)^{1/2}. \quad (18)$$

For a Sun-like star with a core temperature of $T_* = 1.5 \times 10^7$ K, core density $\rho_* = 150 \text{ g/cm}^3$, and DM mass of 100 GeV, this cloud is of the size of ~ 1000 km. For a typical old NS, the thermal radius is $r_{\text{th}} \sim 20$ cm at temperature 10^5 K.

2.2. Signatures of DM in Compact Stars

We have seen, in the previous section, that, even though the DM may accumulate in stars, its total amount may only constitute a tiny fraction $\lesssim 10^{-10}$ of the stellar mass. It may nevertheless produce a number of potentially observable signatures, particularly in compact stars. We discuss below two of these signatures: the heating of NSs by DM annihilations, and destruction of the star by DM collapse into a small BH inside the star.

2.2.1. Annihilation and Heating

Because of a very long DM lifetime, the decay of the accumulated DM can be safely ignored. In many conventional DM models, however, the DM particles can annihilate into the standard model ones. The annihilation rate is proportional to the square of the DM density which is many orders of magnitude higher for DM accumulated inside the star compared to the Galactic DM density. The annihilation may therefore be efficient even for very low annihilation cross sections, particularly for NSs where the accumulated DM concentrates in a very small central region. These annihilations produce heat. In the case of a main sequence star, this heat is smaller compared to energy release of nuclear reactions by at least several orders of magnitude (cf. Equations (7)–(9) with $f \ll 1$) and is therefore negligible. On the contrary, NSs have no major internal heat source; the heat produced by DM annihilations can in principle be detectable [12,34].

In principle, depending on the structure of the dark sector, DM annihilations amplified by its concentration in neutron stars may produce more specific signatures. For instance, it has been pointed out in Ref. [35] that, if DM annihilates into sufficiently long-lived particles that can escape from the neutron star and decay outside into the visible sector, the existing experiments such as Fermi and HESS may impose constraints on the DM parameters several orders of magnitude better than those from the direct detection experiments. Here, we concentrate on the more model-independent heating signature.

In case of annihilation, the current amount of DM in a star is determined by the balance between the accretion and annihilation (for DM masses larger than ~ 10 GeV that we consider here, the evaporation is negligible; for smaller masses, see Ref. [36]). In this case, the number of DM particles in a star $N(t)$ is governed by the equation

$$\frac{dN(t)}{dt} = F - C_A N(t)^2, \quad (19)$$

where, as before, F is the accretion rate and $C_A = \langle \sigma_A v \rangle / V$ is the thermal averaged annihilation cross section σ_A divided by the annihilation volume V . The solution to this equation asymptotes to a constant over the time scale $\tau = 1/\sqrt{FC_A}$. This time scale is typically very short: for a characteristic value of $\langle \sigma_A v \rangle \sim 10^{-26} \text{ cm}^3/\text{s}$ and the rate of Equation (11) taken at $f = 1$, one finds $\tau \sim 10^{-4}$ yr. For the cross sections as low as $\langle \sigma_A v \rangle \gtrsim 10^{-46} \text{ cm}^3/\text{s}$, this timescale is still below 1 Myr [34]. In the equilibrium when the annihilation and capture rates exactly balance each other, the power produced by the annihilation is given simply by the mass accretion rate of Equation (11).

In the absence of other heat sources, the ultimate NS surface temperature is determined by equating the mass capture rate (11) to the black body radiation from the star surface $L = 4\pi R_*^2 \sigma_B T^4$ where σ_B is the Stephan–Boltzmann constant. This gives

$$T = \left(\frac{mF}{4\pi R_*^2 \sigma_B} \right)^{1/4} \sim 5000 \text{ K.} \quad (20)$$

In the absence of annihilations, an NS would cool down below this temperature in about 2×10^7 yr. Having observed an old NS with surface temperature in or below this range would thus impose constraints on the DM annihilation cross sections. Depending on the observed NS temperature and on the DM density at the star location cross sections, a few orders of magnitude below the current direct detection limit may be constrained in this way.

An important observation has been made in Ref. [37] where it was noted that capture of DM particles by the NS itself provides a heat source comparable in power to that of DM annihilations. The gravitational potential inside the NS is 0.2–0.3, so capturing a DM particle releases a sizeable fraction of its rest mass in the form of thermal energy. This energy source is therefore only a factor of a few less efficient than annihilations. This mechanism, referred to as ‘kinetic heating’, is completely free from the assumptions about the DM annihilation cross section. The constraints on the DM from the kinetic heating have been worked out in detail in Refs. [21,38–41].

Internal heating can also be important for WDs. This was recently analysed in [42]. These authors studied the case of relatively light weakly interacting massive particles thermalized in compact objects and compared theoretical predictions on additional luminosity with observations of 10 WDs in a globular cluster M4. In the mass range $\sim 0.1\text{--}5$ GeV, the limit on the cross section of DM particles on baryons is $\sigma_{\text{DM-n}} \lesssim \text{few } 10^{-41} \text{ cm}^2$.

A more complicated model of DM annihilation (with formation of metastable mediators decaying into photons) in application to WDs from the same globular cluster M4 was presented in [43]. Mediators can decay to γ -photons outside a WD, thus this emission can be detected. If mediators decay inside a WD, then an additional contribution to its thermal luminosity appears. Both variants were discussed in [43] and compared with limits on the thermal luminosity of WDs in M4. This allows for putting some model-dependent constraints on the lifetime of mediators.

In principle, the arguments based on the NS heating by DM can be inverted and used to search for DM. In practice, however, the discovery potential of this method is limited by the potential presence of alternative heat sources in old NSs [44,45]. Other DM-related effects may help to overcome this difficulty [46–52].

2.2.2. BH Formation and Star Destruction

Another potential signature of DM accumulation in stars is related to its possible collapse into a small seed BH inside the star with the subsequent accretion of the stellar matter and the star destruction. In order to collapse, the DM has to be concentrated in a small volume. Only models with non-annihilating DM (e.g., asymmetric DM models [53,54]) are relevant in this context as even a tiny annihilation cross section is enough to burn out the accumulated DM. The size of the DM cloud inside the star depends on the stellar core density and is many orders of magnitude smaller for compact stars than for Main sequence ones. We concentrate here on NSs and WDs as providing most favorable conditions for the collapse.

The arguments based on the DM collapse into a BH inside compact stars can be used in both directions: an observation of a NS or a WD in a given DM-rich environment would exclude/constrain those DM models/parameters for which a BH should have been formed inside a WD/NS and converted it into a (sub)solar mass BH. Alternatively, in models where this destruction could take place only in some particularly favorable conditions, one predicts the existence of (sub)solar mass BHs which are not formed by conventional stellar evolution mechanisms.

The general stages of the DM collapse inside a star are as follows. The captured DM forms the cloud of radius given by Equation (18) in the center of the star. As the DM accumulates, its mass density grows and at some point becomes larger than the density of the stellar matter. At this point, the cloud becomes self-gravitating and starts to collapse. As the cloud becomes more strongly bounded, the released energy is evacuated through the collisions with the star nucleons. The shrinking continues either until the extra source of pressure arises that can stabilize the DM sphere, or until the BH is formed in the absence of such a source.

At this last stage, the details of the collapse depend on the DM nature—whether it is bosonic or fermionic. In the case of free fermions, the Fermi pressure will halt the collapse unless the number of particles is sufficiently large. The required number of DM particles is given by an analog of the famous Chandrasekhar condition which in the case at hand reads:

$$N_{\min,f} \sim \left(\frac{M_{\text{Pl}}}{m}\right)^3 = 2 \times 10^{51} \left(\frac{100 \text{ GeV}}{m}\right)^3. \quad (21)$$

Note that, for $m \sim 1 \text{ GeV}$, this equation roughly reproduces the number of neutrons in a NS. In case of free bosons, this is the quantum uncertainty principle that halts the collapse if the number of particles is smaller than

$$N_{\min,b} \sim \left(\frac{M_{\text{Pl}}}{m}\right)^2 = 2 \times 10^{34} \left(\frac{100 \text{ GeV}}{m}\right)^2. \quad (22)$$

The required number of particles in this case is much smaller than in the case of fermions. Note, however, that Equation (22) assumes that bosons are non-interacting; interactions may significantly modify this equation as will be discussed below.

Consider first the case of free fermions. In this case, the number of DM particles required to make a BH is given by Equation (21). Let us compare it to the number that can be accumulated according to Equation (11). Assuming the NS lifetime of 1 Gyr Equation (11) implies the total accumulated amount of $8 \times 10^{42} \text{ GeV}$ in the conditions typical for the Milky Way, regardless of the DM mass. Dividing by the mass and requiring that the resulting number is larger than that of Equation (21), one finds the condition

$$m \gtrsim 10^7 \text{ GeV}, \quad (23)$$

in agreement with the results of Ref. [28]. The DM models with heavier fermionic DM would then contradict observations of NS in the Milky Way, provided the DM has a scattering cross section on neutrons that are larger than $\sigma \gtrsim 10^{-45} \text{ cm}^2$ so that Equation (11) is valid with $f = 1$.

This constraint on the mass can be improved by excluding lower DM masses in two ways. The minimum mass to form a BH scales like the square root of the capture rate. The latter, in turn, scales like ρ_{DM}/\bar{v} . Observation of NSs in DM-rich environments thus leads to stronger constraints. For instance, in dwarf galaxies, both the DM density is higher by a factor up to ~ 200 , and the velocity of DM particles is lower by up to 30 times. Thus, in dwarf galaxies, the capture rate may be higher by nearly four orders, and correspondingly the constraints on the fermionic DM mass start at masses lower by 1.5–2 orders of magnitude compared to Equation (23). The second improvement may be achieved by taking into consideration the accumulation of DM by the NS progenitor. The efficient accumulation of DM in the Main sequence stars requires large DM-nucleon cross section in view of Equations (3). The argument, therefore, applies to models with the spin-dependent DM-nucleon cross section that is less constrained. Depending on the value of this cross section, masses as low as $\sim 10 \text{ TeV}$ can be potentially constrained [27].

We have considered so far non-interacting fermions. Adding self-interactions may change the collapse conditions. The simplest Yukawa interaction with the scalar mediator gives the attractive interaction which may reduce the number of DM particles required for

the collapse [55–57]. Note, however, that the non-relativistic approximation becomes inadequate in the relativistic regime close to the collapse [58], which may limit this reduction to a mere factor of a few as compared to the non-interacting case.

Let us turn now the case of bosonic DM. In the case of bosons, one more phenomenon has to be taken into account, the formation of the Bose–Einstein condensate (BEC) [59]. The condition for the BEC formation (large phase space density) can be formulated in terms of DM number density n and the star core temperature T_c and reads

$$n \gtrsim 5 \times 10^{28} \text{ cm}^{-3} \left(\frac{m}{\text{GeV}} \right)^{3/2} \left(\frac{T_c}{10^5 \text{ K}} \right)^{3/2}, \tag{24}$$

where we assumed that DM particles are in thermal equilibrium with the star. In view of Equation (11), this condition becomes satisfied very quickly. Once the BEC is formed, newly captured DM particles go into the condensed state. The size of the condensate d is determined by the size of the lowest quantum level of DM in the gravitational potential of the NS:

$$d = \left(\frac{8\pi}{3} G \rho_c m^2 \hbar^{-2} \right)^{-1/4} \sim 2 \times 10^{-4} \text{ cm} \left(\frac{\text{GeV}}{m} \right)^{1/2}, \tag{25}$$

where ρ_c is the star core density. This size is much smaller than the size of the thermal DM cloud. Because of the small size of the BEC, the density of DM in the BEC quickly exceeds the density of nucleons in the star. This happens when the accumulated DM mass becomes larger than

$$M \gtrsim 10^{28} \text{ GeV} \left(\frac{m}{\text{GeV}} \right)^{-3/2}, \tag{26}$$

i.e., almost immediately after the star formation. The self-gravitating BEC then grows until the condition of BH formation is satisfied.

In the case of zero DM self-interactions, there is nothing that can stop the BH formation once the number of DM particles exceeds that given in Equation (22). In this case, the constraints can be imposed on the DM parameters. Requiring that the BH that is formed is heavy enough to grow by accretion faster than it evaporates by the Hawking radiation, one may exclude the DM masses in the range 100 keV–10 GeV for DM-nucleon cross sections at the current experimental limit [59,60]. For heavier masses, the BH formed in the DM collapse is too light and evaporates through Hawking radiation faster than it accretes the matter of the star [61] with no observable consequences apart from heating of the star as already discussed above. Adding even a tiny $\lambda\phi^4$ self-interactions shifts the exclusion region into the multi-TeV range (see Figure 2 of [59]). A detailed recent analysis of these constraints can be found in [31].

It has been pointed out in Ref. [62] that self-interactions must be present at a non-negligible level, the reason being as follows. Even if a direct coupling between DM particles is not included in the Lagrangian, the DM interactions with nucleons that are necessary for capture will induce the DM-DM self-interactions in the higher orders of perturbation theory. There is, however, a subtlety in this argument. The DM-nucleon scattering which is necessary for capture occurs at low energies, while the DM-DM self-interactions present an obstacle for collapse at very high (Planckian) values of fields. These two scales are not necessarily related. Thus, while it is easy to avoid the constraints by adding an appropriate DM self-interaction, the assumption that self-interactions are negligible at the collapse is not in contradiction with the non-zero DM interaction with nucleons at low energies.

Having excluded some regions of the DM parameter space by NS implosions due to formation of seed BHs automatically implies, by continuity that, for the parameters close to those regions but not excluded, one may look for signatures of these implosion events. These signatures may include particular gravitational wave events [63–66], quiet kilonovae [64], supernovae [67–69], an impact on star population [70], and existence of (sub)Solar-mass BHs [57,71] not expected to result from conventional stellar evolution mechanisms.

3. Axions and Neutron Star Magnetospheres

3.1. Theory

One of the unsolved issues of the Standard model (SM) of particles is a strong CP problem, i.e., absence of CP-violation in the quantum chromodynamics (QCD). The theory contains terms that could generate CP-violation, so extreme closeness of parameter θ that describes strength of the violation and could take values anywhere in $[0, 2\pi]$ interval to zero seems unnatural. One of the most elegant solutions of the strong CP problem was suggested by Peccei and Quinn ([72])—to treat θ as a new dynamical field, rather than a fixed parameter. Dynamics of this field could drive the value of CP-parameter to zero, effectively solving the problem. There also would be particles corresponding to this field—axions [73,74]. There is no unique way to add axion to the SM, and two of the most popular models are KSVZ (Kim–Shifman–Vainshtein–Zakharov) and DFSZ (Dine–Fischler–Srednicki–Zhitnitsky) [75–78] which predict couplings of axion to SM particles of similar strengths and frequently serve as benchmarks. In these models, the axion mass m_a is a free parameter that can change in a very wide range and should be found from experiments. One of the general predictions for axions is that their coupling constants, e.g., the coupling constant to photons $g_{a\gamma\gamma}$, are proportional to mass m_a , meaning that less massive axions become progressively more elusive for direct or indirect detection. Still, it is at least theoretically possible to reach this line, or, given uncertainties, band on $m_a - g_{a\gamma\gamma}$ plane for some values of m_a and therefore test the model of QCD axion in a certain mass range. In low-energy effective field theories derived from some string models, a more general class of axion-like particles (ALPs) could emerge (e.g., [79–81]). For ALPs, mass and coupling constants are independent.

Axions (and ALPs) are also regarded as a possible DM candidate [82,83]. Though they are very light by standards of WIMPs, with masses < 1 eV, still axions could contribute to cold DM (CDM). A concise review of axion and ALPs and present the status of different experiments searching for them could be found in [84]. Properties of axions and ALPs which are relevant to us are very close, so, from now on, we will refer to both of them as axions. Throughout this section, we use units with $\hbar = c = 1$ and $\alpha = e^2/4\pi \approx 1/137$.

Most of the search methods rely on the very weak axion coupling to photons. The Lagrangian of the axion–photon system in a vacuum without QED corrections is described as follows:

$$\mathcal{L} = -\frac{1}{4}F_{\mu\nu}F^{\mu\nu} + \frac{1}{2}(\partial_\mu a\partial^\mu a - m_a^2 a^2) + \frac{1}{4}g_{a\gamma\gamma}aF_{\mu\nu}\tilde{F}^{\mu\nu}, \tag{27}$$

where $F_{\mu\nu} \equiv \partial_\nu A_\mu - \partial_\mu A_\nu$ is the electromagnetic field tensor, $\tilde{F}^{\mu\nu} \equiv \frac{1}{2}\epsilon_{\mu\nu\rho\sigma}F^{\rho\sigma}$ is its dual, and a, m_a are the axion field and mass, respectively. The coupling term could be rewritten using magnetic and electric fields strengths \vec{E}, \vec{B} : $\frac{1}{4}g_{a\gamma\gamma}aF_{\mu\nu}\tilde{F}^{\mu\nu} = \frac{1}{4}g_{a\gamma\gamma}a\vec{E} \cdot \vec{B}$. The equations of axion electrodynamics could be derived from the Lagrangian (27) [85,86]:

$$\nabla \cdot \vec{E} = -g_{a\gamma\gamma}\vec{B} \cdot \nabla a, \tag{28}$$

$$\nabla \times \vec{E} = -\frac{\partial \vec{B}}{\partial t}, \tag{29}$$

$$\nabla \cdot \vec{B} = 0, \tag{30}$$

$$\nabla \times \vec{B} = \frac{\partial \vec{E}}{\partial t} + g_{a\gamma\gamma}\dot{a}\vec{B} + g_{a\gamma\gamma}\nabla a \times \vec{E}, \tag{31}$$

$$\square a + m_a^2 a = g_{a\gamma\gamma}\vec{E} \cdot \vec{B}. \tag{32}$$

Let us assume that there is some background magnetic field \vec{B}_0 and perturbations \vec{E}, \vec{B} propagating over it. In most astrophysical scenarios, a background electric field \vec{E}_0

could be safely set equal to zero. Furthermore, as we deal with propagating EM waves, it is sufficient to describe E -component only:

$$\square \vec{E} + \nabla(\nabla \cdot \vec{E}) = -g_{a\gamma\gamma} \ddot{a} \vec{B}_0. \tag{33}$$

$$\square a + m_a^2 a = g_{a\gamma\gamma} \vec{E} \cdot \vec{B}_0. \tag{34}$$

It is illuminating to consider the simplest setup: the EM wave and axion propagate along the z -axis in a static and uniform background magnetic field \vec{B}_0 . As the coupling is sourced by the scalar product $\vec{E} \cdot \vec{B}_0$, only a transverse component of the magnetic field \vec{B}_0 enters into the equations of motion—we use it to define the direction of x -axis. In addition, only one polarization $E_{||} = E_x$ couples to axion and experiences conversion to axion and vice versa, as, for the other one, the scalar product $\vec{E} \cdot \vec{B}$ vanishes.

Factorizing out temporal dependence $\sim e^{i\omega t}$, we arrive at the following set of equations:

$$\begin{pmatrix} \omega^2 + \partial_z^2 - m_a^2 & \omega g_{a\gamma\gamma} B(z) \\ \omega g_{a\gamma\gamma} B(z) & \omega^2 + \partial_z^2 \end{pmatrix} \begin{pmatrix} a \\ E_{||}/\omega \end{pmatrix} = 0 \tag{35}$$

These second-order equations could be solved numerically. Another approach is to linearize them and obtain analytic results from first-order equations. The details of the linearization procedure depend on the dispersion relation for axion $\omega^2 = m_a^2 + k^2$, where k is the wave vector, and slightly differs for cases of relativistic and non-relativistic axion. The former case, which is e.g., relevant for propagation of X-ray photons in magnetospheres of NS, was first thoroughly studied in [87]. For ultrarelativistic axions, $k \approx \omega$ and the linearized equations have a very simple form (for non-relativistic axions, an analogous expression can be found e.g., in [86]):

$$\begin{pmatrix} \omega - i\partial_z - \frac{m_a^2}{2\omega} & \frac{g_{a\gamma\gamma} B(z)}{2} \\ \frac{g_{a\gamma\gamma} B(z)}{2} & \omega - i\partial_z \end{pmatrix} \begin{pmatrix} a \\ E_{||}/\omega \end{pmatrix} = 0 \tag{36}$$

These Schrodinger-like equations describe the behavior of a system of two mixed states. We are mainly interested in a probability of conversion between them. In case of a homogeneous constant magnetic field B , the probability of conversion of one particle into another depends on the travelled distance L [87,88]:

$$P(L) = \frac{g_{a\gamma\gamma}^2 B^2}{m_a^4/4\omega^2 + g_{a\gamma\gamma}^2 B^2} \sin\left(\frac{L\Delta_{osc}}{2}\right), \tag{37}$$

$$\Delta_{osc}^2 = m_a^4/4\omega^2 + g_{a\gamma\gamma}^2 B^2. \tag{38}$$

Photons and axions are in a strong mixing regime, when $g_{a\gamma\gamma} B \gg m_a^2/2\omega$. In this regime, almost a full conversion of photons to axions and back is possible with a characteristic length scale of oscillations $l_{osc} = 2\pi/\Delta_{osc} = 2\pi/g_{a\gamma\gamma} B$. In the opposite case, $g_{a\gamma\gamma} B \ll m_a^2/2\omega$, the amplitude of oscillations is greatly suppressed. This suppression comes from the fact that the phase velocities of waves corresponding to massless photon and massive axion are slightly different and the conversion process has only a limited time to build up while these waves propagate in phase. After that, the conversion process falls out of the resonance, effectively limiting the amplitude of oscillations.

This picture of axion/EM wave propagating in vacuum could be generalized to a more physical scenario. Now, we take into account effects of medium and QED-induced terms which changes the velocity of propagation of EM waves [87,88]. Equation (36) should be rewritten as follows:

$$\begin{pmatrix} \omega - i\partial_z + \Delta_a & \Delta_M \\ \Delta_M & \omega - i\partial_z + \Delta_{||} \end{pmatrix} \begin{pmatrix} a \\ E_{||}/\omega \end{pmatrix} = 0, \tag{39}$$

where $\Delta_a = -\frac{m_a^2}{2\omega}$, $\Delta_M = \frac{g_{a\gamma\gamma} B \sin \Theta}{2}$, and Θ is the angle between the direction of axion propagation and background magnetic field. In astrophysical sources, the mixing term $\Delta_{||}$ is a sum of two parts $\Delta_{||} = \Delta_{pl} + \Delta_{QED,||}$. The first one arises due to the influence of plasma, where the photon acquires effective mass and propagates slower than in a vacuum: $\Delta_{pl} = -\frac{\omega_{pl}^2}{2\omega}$, $\omega_{pl} = \sqrt{\frac{4\pi\alpha n_e}{m_e}}$, α is the fine-structure constant, n_e is the number concentration of electrons, and m_e is the electron charge¹. The second term $\Delta_{QED,||}$ comes from QED-induced corrections and depends on the strength of magnetic field B , $\Delta_{QED,||} = \frac{1}{2}q(b)\omega \sin^2 \Theta$, $q(b)$ is a function of parameter $b \equiv \frac{B}{B_{cr}}$, $B_{cr} = m_e^2/e = 4.4 \times 10^{13}$ G, which can be approximated in the following form [89]:

$$q = \frac{7\alpha}{45} b^2 \hat{q}, \quad \hat{q} = \frac{1 + 1.2b}{1 + 1.33b + 0.56b^2}. \tag{40}$$

Usually, it is sufficient to use the small- b approximation $\Delta_{QED,||} = \frac{7\alpha}{90} \omega \left(\frac{B}{B_{cr}}\right)^2 \sin^2 \Theta$. The only possible exception could arise when one considers the propagation of EM waves in the immediate vicinity of magnetars, where the magnetic field could be considerably higher than B_{cr} . The introduction of these new mixing terms slightly modifies the expression (37) for probability $P(L)$:

$$P(L) = \frac{4\Delta_M^2}{(\Delta_{pl} + \Delta_{QED,||} - \Delta_a)^2 + 4\Delta_M^2} \sin\left(\frac{L\Delta_{osc}}{2}\right), \tag{41}$$

$$\Delta_{osc}^2 = (\Delta_{pl} + \Delta_{QED,||} - \Delta_a)^2 + 4\Delta_M^2. \tag{42}$$

It can be seen that now it is possible for photons and axions to experience very efficient conversion when the resonance condition $(\Delta_{pl} + \Delta_{QED,||} - \Delta_a) = 0$ is met. This effect is used in radio searches for axions both in laboratory and in observations of compact stars (see Section 3.3 below). On the other hand, as $\Delta_{QED,||}$ and Δ_a have different signs, a QED-induced term can further suppress conversion, comparing to the vacuum case. This is relevant for propagation of X-ray photons and axions of corresponding energies in magnetospheres of MWDs and NSs.

To conclude this section, we will present some benchmark values for the mixing terms, using typical values for relevant parameters:

$$\begin{aligned} \Delta_a &= -\frac{m_a^2}{2\omega} = -5 \times 10^{-16} \left(\frac{m_a}{1 \mu\text{eV}}\right)^2 \left(\frac{\omega}{1 \text{ keV}}\right)^{-1} \text{ eV} = \\ &= -2.538 \times 10^{-11} \left(\frac{m_a}{1 \mu\text{eV}}\right)^2 \left(\frac{\omega}{1 \text{ keV}}\right)^{-1} \text{ cm}^{-1}, \end{aligned} \tag{43}$$

$$\begin{aligned} \Delta_{pl} &= -\frac{\omega_{pl}^2}{2\omega} = -\frac{2\pi\alpha n_e}{m_e\omega} = \\ &= -6.87 \times 10^{-15} \left(\frac{n_e}{10^{10} \text{ cm}^{-3}}\right)^2 \left(\frac{\omega}{1 \text{ keV}}\right)^{-1} \text{ eV} = \\ &= -3.48 \times 10^{-10} \left(\frac{n_e}{10^{10} \text{ cm}^{-3}}\right)^{-1} \left(\frac{\omega}{1 \text{ keV}}\right)^{-1} \text{ cm}^{-1}, \end{aligned} \tag{44}$$

$$\begin{aligned} \Delta_M &= \frac{g_{a\gamma\gamma} B \sin \Theta}{2} = 9.76 \times 10^{-10} \left(\frac{g_{a\gamma\gamma}}{10^{-10} \text{ GeV}^{-1}}\right) \left(\frac{B}{10^{12} \text{ G}}\right) \sin \Theta \text{ eV} = \\ &= 4.94 \times 10^{-5} \left(\frac{g_{a\gamma\gamma}}{10^{-10} \text{ GeV}^{-1}}\right) \left(\frac{B}{10^{12} \text{ G}}\right) \sin \Theta \text{ cm}^{-1}, \end{aligned} \tag{45}$$

$$\begin{aligned} \Delta_{QED,||} &= \frac{7\alpha}{90} \omega \left(\frac{B}{B_{cr}}\right)^2 \sin^2 \Theta = \\ &= 9.33 \times 10^{-5} \left(\frac{B}{10^{12} \text{ G}}\right)^2 \left(\frac{\omega}{1 \text{ keV}}\right) \sin^2 \Theta \text{ eV} = \\ &= 4.73 \left(\frac{B}{10^{12} \text{ G}}\right)^2 \left(\frac{\omega}{1 \text{ keV}}\right) \sin^2 \Theta \text{ cm}^{-1}. \end{aligned} \tag{46}$$

Relative strength of these terms defines which effect dominates during propagation. In realistic situations where the field is inhomogeneous, the probability is calculated by numerical integration of Equations (39) from some starting point to infinity [87]:

$$P_{a \rightarrow \gamma} = \left| \int_{R_0}^{\infty} dr' \Delta_M(r') e^{i\Delta_a r' - i \int_{R_0}^{r'} dr'' \Delta_{QED,||}(r'')} \right|^2. \tag{47}$$

3.2. Hot Axions

Extremely strong magnetic fields around NSs naturally make them obvious targets for searches for signatures of axion–photon oscillations. First, it was suggested to search for high-energy X-ray photons from conversion of axions produced in cores of NSs [87,90]. The temperature in central parts of these objects can reach extremely high values, $T_c \sim 10^9$ K, and the axions could be generated there in the bremsstrahlung process during interactions of nucleons, $n + n \rightarrow n + n + a$. These axions would propagate freely in the interiors of the NS but could convert in the external magnetic fields into energetic photons that could be easily distinguished from thermal photons coming from the surface as its temperature is much lower, $T_s \sim 10^6$ K. The inverse process of photon to axion conversion could also lead to the emergence of potentially observable spectral and polarization features in X-ray and other energy ranges [91–93].

At $\mathcal{O}(\text{keV})$ energies, conversion takes place in a weak mixing mode almost everywhere, as could be seen from Equations (46), and the dominating term is $\Delta_{QED,||}$. Particles could still experience photon–axion resonance, when resonance condition $\Delta_{pl} + \Delta_{QED,||} - \Delta_a = 0$ is met. This is possible when $\Delta_{pl} \approx -\Delta_{QED,||}$, which defines corresponding density [91]:

$$\rho_{res} = 2.25 \times 10^{-4} \frac{1}{Y_e} \left(\frac{B}{10^{12} \text{ G}} \right)^2 \left(\frac{\omega}{1 \text{ keV}} \right)^2 \text{ g cm}^{-3}, \tag{48}$$

where Y_e is the electron fraction. In resonance, the photon–axion system is in the strong mixing regime, and it is theoretically possible to obtain complete conversion from one state to another. However, the needed oscillation length $l_{osc} = \frac{\pi}{\Delta_M}$ is much larger than the characteristic scale of the NS atmosphere $h_{atm} \sim \mathcal{O}(10)$ cm, let alone a more narrow region where density is close to the value which makes the resonance possible. Because the contribution from the resonance conversion is subdominant, and in all calculations of conversion probability, it is possible to neglect the plasma term Δ_{pl} .

Hot axions generated in the centers of NSs have a modified thermal distribution [94,95] with spectrum peaking around $E_{peak} \sim 3.3T_c$ and for temperatures $T_c \sim 10^9$ K the flux is non-negligible in a 10–1000 keV energy range. It is customary to calculate the probability of conversion using Equation (47) assuming a simple dipolar model for an NS magnetic field and purely radial propagation [96,97]. This probability could be estimated as follows [97]:

$$P_{a \rightarrow \gamma} = 6 \times 10^{-3} \left(\frac{g_{a\gamma\gamma}}{10^{-10} \text{ GeV}^{-1}} \right)^2 \left(\frac{B}{10^{12} \text{ G}} \right)^{2/5} \left(\frac{\omega}{1 \text{ keV}} \right)^{-4/5} \left(\frac{R_{NS}}{10 \text{ km}} \right)^{6/5}. \tag{49}$$

Multiplying the theoretically expected axionic spectrum by the probability, it is now possible to obtain the spectrum of X-rays from the conversion and compare it to observations. In addition, polarization measurements could be used to constrain properties of axions: converted photons could have only single polarization $E_{||}$, also known as O-mode (ordinary), while many models of NS atmospheres predict that NS emission, especially at lower energies <1 keV, is primarily polarized in perpendicular X-mode (extraordinary) [98] and an admixture of a differently polarized mode could be, in principle, detected [99].

Different classes of NSs were suggested to use for this type of searches. First, the magnetars [96,99]—NSs with extremely high magnetic fields exceeding 10^{14} G and high central temperatures, up to $\sim 10^9$ K, which boosts their axionic luminosities. There are obvious downsides as well: all of them are rather distant and that greatly decreases the flux observed at the Earth. In addition, these objects demonstrate high-energy activity which makes it non-trivial to disentangle possible contribution from axion–photon oscillations. Nevertheless, the observations of magnetars in the energy range 10–1000 keV allowed for putting meaningful constraints on the product of couplings $g_{a\gamma\gamma} \times g_{ann}$ [100,101]. The most stringent constraints come from magnetar 1E 1547.0-5408: $g_{a\gamma\gamma} \times g_{ann} < 4.4 \times 10^{-20} \text{ GeV}^{-1}$ for $T_c = 10^9$ K.

Another interesting set of candidates are X-ray dim isolated NSs (XDINSs, also known as the Magnificent Seven) (e.g., [102]). These NSs are detected mainly in X-rays (plus, dim optical counterparts are known for most of them), and their emission is thought to originate at their surfaces with spectra which are very close to blackbody with temperatures $T_s \sim 0.1$ keV. Detected evolution of spin periods allowed for inferring magnetic fields of these objects: $B \sim 10^{13}$ G which makes a quite effective conversion possible. Their relative proximity to the Earth, with distances in a 100–600 pc range, also benefits searches. Deep observations in a 2–8 keV range by XMM-Newton and Chandra revealed the existence of X-ray excess for two XDINS: RX J1856.6-3754 and RX J0420.0-5022 [103]. This excess could be explained by axion–photon conversion if $g_{a\gamma\gamma} \times g_{ann} \sim 4.0 \times 10^{-20} \text{ GeV}^{-1}$ (only a central value is quoted, systematic and statistical uncertainties could exceed an order of magnitude) [97]. This value is only slightly lower than one coming from a combination of constraints from CAST helioscope on $g_{a\gamma\gamma}$ and from SN 1987A on g_{ann} , so it is possible that this result would soon be tested with new experiments such as IAXO.

Photon to axion conversion and induced changes in observed spectrum and polarization of NS X-ray emission was extensively studied in [93]. Although the possible constraints depend now only on $g_{a\gamma\gamma}$ coupling, the theoretical uncertainties in modeling of NS atmospheres greatly complicate the task of setting them. Usually, it is assumed that below 1–2 keV intrinsic emission of the NS is X-polarized due to an increased opacity for O-mode. As the X- and O- mode could convert into each other in a process similar to axion–photon conversion [91,93], the emission is mostly polarized in O-mode at higher energies—originally produced X-polarized photons experience conversion into O-photons in so-called vacuum resonance. Vacuum and axion–photon resonances occur at well separated regions, so it is possible to treat them independently and, instead of a three-state system (X, O, axion) study, consequently, two two-state systems (O, axion) and (X, O) [91]. It was shown that, if the photons come from hot spots rather than the entire surface, their conversion to axions would lead to phase-dependent suppression of a high-energy tail of the spectrum [93]. In the opposite case, the conversion would affect the inferred radius of NS which could lead to contradictions with values found by other methods.

Another possible way to use photon to axion conversion was suggested recently in [104]—optical photons emitted from the surface of XDINS should also follow blackbody distribution with temperature that can be inferred from X-ray observations of these objects. Conversion into axions would lead to dimming in the optical part of the spectrum, which theoretically allows for probing coupling constraints down to values $g_{a\gamma\gamma} \sim 10^{-11} \text{ GeV}^{-1}$.

Further observational progress would be reached with a new generation of X-ray telescopes: Athena [105] would reach the level of sensitivity which would make possible phase-resolved observations of XDINSs and magnetars. Effectiveness of the axion–photon conversion process varies with a rotational phase due to changing orientation of the magnetic field, so these observations could make a crucial contribution to the field. In addition, polarimetric observations with telescopes like XIPE [106] would significantly further our progress in understanding of NS atmospheres and propagation of X-ray photons in them, thus allowing for putting stronger constraints on axion properties.

3.3. Compact Object as Haloscopes

Another promising method of axion detection was initially suggested in [107]. If the axions are the main DM component, than their conversion in strong magnetic fields of NS magnetosphere could be possibly revealed by the presence of sharp spectral feature, similar to the laboratory haloscopes used to search for axions (e.g., ADMX [108]).

Flux of axions through magnetosphere is enhanced by gravitational focusing and infalling particles travelling through the inner regions of the magnetosphere have a chance to convert into photons. In this case, we are dealing with a conversion of non-relativistic axions, so the resulting signal would be almost monochromatic at the frequency corresponding to axion mass m_a with a certain shift and widening due to the Doppler effect.

Renewed interest in this method of axion searches led to fast progress in our understanding of the details of the process [86,109–114]. The conversion process is slightly different for non-relativistic axions: governing linearized equations are altered [86], and conversion occurs in a resonant mode, in a stark contrast to conversion of ‘hot’ axions, as discussed above. In addition, plasma effects that influence propagation of EM waves are much more important for the conversion of non-relativistic axions [113,114].

One of the main properties that directly affects potential sensitivity of radio observations is the resulting width of the radio line. It is mostly defined by interaction of infalling axions with rotating plasma of an NS magnetosphere [86] and can reach values as high as:

$$\frac{\delta f}{f} \sim \mathcal{O}\left(\frac{\Omega r_c}{c}\right) = 6 \times 10^{-4} \left(\frac{\Omega}{1 \text{ Hz}}\right) \left(\frac{r_c}{200 \text{ km}}\right), \quad (50)$$

where r_c is the critical radius where conversion takes place, $\omega_{pl}(r_c) = m_a$. This contribution due to Doppler broadening strongly dominates over one caused by DM particle velocity dispersion \bar{v} :

$$\frac{\delta f_{disp}}{f} = \frac{\bar{v}^2}{2c^2} = 8 \times 10^{-7} \left(\frac{\bar{v}}{100 \text{ km s}^{-1}}\right)^2.$$

More rigorous treatment of 3D propagation in plasma, including the ray-tracing technique, lead to modification of the magnitude of the expected effect, when compared to simple 1D calculations. 3D non-radial trajectories of photons, unlike axions, are not rectilinear and that in turn leads to de-phasing and suppression of resonance, which results in somewhat lower flux from conversion [113]. In addition, plasma effects could lead to emergence of a rich temporal structure of a signal.

Due to their proximity and relatively high magnetic fields, XDINSs are again considered to be very good observational targets for searches in the radio domain. Observations of RX J0720.4-3125 and RX J0806.4-4123 with a Green Bank radio telescope found no excess signal and that allowed for setting constraints: $g_{a\gamma\gamma} < 10^{-11} \text{ GeV}^{-1}$ for $5.5 < m_a < 7.0 \text{ } \mu\text{eV}$ [115].

Signals from NSs could be greatly increased if they reside in regions with enhanced DM density. Another candidate that potentially could lead to even more stringent constraints is magnetar PSR J1745-2900 with $B \approx 1.6 \times 10^{14} \text{ G}$, which is only 0.1 pc away from the central supermassive black hole Sgr A*. The boost factor which can be defined as ratio of DM density at the NS position relative to DM density near the Solar system $\eta = \rho_{DM}/\rho_{DM,\odot}$ could reach 1.5×10^5 in a Navarro–Frenk–White (NFW) model of the DM halo and could exceed 10^9 in models with a spike near the SMBH. This object was extensively studied using Effelsberg observations [115] and archival data from Karl G. Jansky Very Large Array [116–118]. Constraints can be set in several broad windows from 4 to 160 μeV , which correspond to radiotelescope frequency bands spanning from 1 to 40 GHz. Assuming NFW model [119] constraints can reach the $g_{a\gamma\gamma} < 10^{-11} \text{ GeV}^{-1}$ level, while they could be two orders of magnitude stronger if there was a DM spike around the SMBH. At the moment, the greatest uncertainty comes from our limited knowledge of DM distribution near the Galactic center. In the future, supreme sensitivity of the SKA would allow for testing couplings as small as $g_{a\gamma\gamma} \sim 10^{-13} \text{ GeV}^{-1}$ even assuming the NFW model [113].

MWDs could also be possible targets of observations, as the conversion of DM could analogously take place in their magnetospheres. In [120], it was shown that future observations of MWD 2010+310 with SKA phase 1 can probe coupling as low as $g_{a\gamma\gamma} \sim 10^{-12} \text{ GeV}^{-1}$ in a 0.2–3.7 μeV mass range.

3.4. Axions and FRBs

Fast radio bursts (FRBs) are extragalactic radio flares with millisecond duration discovered by [121]. The question of their origin is one of the major astrophysical mysteries nowadays (see reviews, e.g., in [122–124]). Axion to photon conversion in a strong magnetic field was one of the first scenarios involving astroparticle physics.

A sizable fraction of axions constituting DM could undergo the process of condensation, forming relatively dense clusters with masses $\sim \mathcal{O}(10^{-12} M_{\odot})$ and characteristic sizes of $\sim \mathcal{O}(100 \text{ km})$. If, during a passage through a magnetosphere of an NS, such cluster experiences partial or full conversion and the axion mass falls in the $\mathcal{O}(\mu\text{eV})$ range, there would be a bright short radio flare. Conversion of $\sim \mathcal{O}(10^{-13}–10^{-12} M_{\odot})$ into EM radiation could have explained outstanding energetics of FRBs with total emitted energy reaching $E_{tot} = 10^{40}$ ergs [125,126].

As it was quickly demonstrated, this simplified scenario could not work as axion miniclusters are too loosely bound and would be destroyed by tidal forces long before they could reach the region of efficient conversion and so duration of the resulting flare would be on the order of seconds rather than milliseconds [127]. However, accurate treatment of equations, describing axion condensation shows that there is a branch of solutions, which correspond to much more concentrated objects, dubbed dense axion stars. With masses around $10^{-13} M_{\odot}$ but characteristic sizes less than about a meter, they are immune to forces of tidal disruption and could reach region of resonant conversion intact [128,129]. Thus, it is still possible that some sub-population of FRBs could be explained by this process.

4. Axions and Cooling of White Dwarfs

Already in 1986 it was proposed that axions can be emitted by WDs due to the bremsstrahlung process when electrons scatter off nucleons (or nuclei) [130]. This additional energy loss might contribute to WD cooling and thus can be detected (directly or indirectly) by different methods. Since the publication of the original idea (when some constraints on the axion parameters have been made already), many researchers advanced this approach in many ways. In this section, we present and summarize the main recent results in this field of astroparticle physics trying to mention different methods of constraining axion parameters via astronomical observations involving WDs.

The first approach is quite similar to the one described in Section 3 above for the case of NSs. Axions emitted in hot and dense WD interiors can be converted to photons in strong magnetic fields of MWDs [131] (see therein references to earlier similar ideas in application to other types of astronomical sources). In MWDs, the surface field can reach 10^9 G [132]. Such strong field axions can turn to X-ray photons via the already discussed above Primakoff effect. Production of X-ray emission is related to the fact that temperatures at WDs interiors can be of the order of 10^7 K . In comparison with NSs, WDs have one important advantage: their surface temperatures are too low to produce significant flux of thermal X-ray photons of keV energy. Thus, all detected photons can be related to the conversion of axions.

Expected luminosity is non-negligible; in [131], the authors provide the following estimate:

$$L_{ax} = 1.6 \times 10^{-4} \left(\frac{g_{aee}}{10^{-13}} \right)^2 \left(\frac{M}{1 M_{\odot}} \right) \left(\frac{T_c}{10^7 \text{ K}} \right)^4 L_{\odot}. \quad (51)$$

Here, M is WD mass, and T_c is its central temperature. If all axions are converted to X-ray photons in the WD's magnetosphere, this would correspond to flux $\approx 5 \times 10^{-13} d_{100}^{-2} \text{ erg cm}^{-2} \text{ s}^{-1}$, where d_{100} is a distance normalized to 100 pc (we neglect interstellar absorption, which is reasonable for near-by sources in keV range). Such fluxes are well within reach by modern

X-ray observatories like Chandra or XMM-Newton, and, in the future Athena, will bring many more examples. Of course, conversion efficiency is far from ideal. Still, X-ray data on MWD RE J0317-853 obtained with Suzaku satellite allowed the authors of [131] to obtain a strong limit on low-mass axions' parameters. Later, dedicated observations of the same source produced even better constraints.

The idea proposed in [131] was recently realized in the study by Dessert et al. [133]. These authors analyzed Chandra observations of MWD RE J0317-853 at ~ 30 pc from the Sun. No X-ray emission was detected. Accurate modeling and usage of recent data allowed for obtaining a better estimate of the central temperature: ≈ 1.4 keV. Altogether, this allowed for placing an upper limit $g_{a\gamma\gamma} \lesssim 5.5 \times 10^{-13} \sqrt{C_{a\gamma\gamma}/C_{aee}} \text{ GeV}^{-1}$. For low-mass axions ($m_a \lesssim 10^{-5}$ eV), this constraint is much better than the one obtained by CAST [134]. Future observations with new generation of space X-ray observatories might allow for increasing this limit substantially, or even to detect the effect. An opposite process—conversion of thermal surface photons to axions in magnetospheres of MWDs—was used by [135] to put stringent limits on $g_{a\gamma\gamma}$ by observation of linear polarization of optical emission from MWDs.

If axions are important for WD cooling, then this effect influences not only individual sources, but also general properties of the whole population of these compact objects. In particular, luminosity distribution of WDs—so-called, luminosity function, $n(L)$ [136]:

$$n(L) = \int_{M_{low}}^{M_{up}} \Phi(M) \Psi(\Delta t) \tau_{cool}(L, M) dM. \quad (52)$$

In this expression, L and M are luminosity and mass of a WD, respectively. $\Phi(M)$ is the initial mass function and $\Psi(t)$ —star formation rate. Characteristic time scale is defined as $\tau_{cool} = dt/dM_{bol}$, where M_{bol} is absolute bolometric magnitude. Finally, M_{up} and M_{low} are stellar masses that define the range of WD formation in a given population. Each stellar mass has one-to-one correspondence with a WD mass.

In Equation (52), time interval Δt is the difference between the age of population under consideration (can be equal to the Galactic age) and sum of the cooling age (time necessary to reach the given luminosity L) and lifetime of the progenitor: $\Delta t = t_{pop} - (t_{cool}(L, M) + t_{pro}(M))$. The minimum progenitor mass can be defined from equation: $t_{pop} = t_{cool}(L, M_{low}) + t_{pro}(M_{low})$ (stars with lower masses had no time to evolve up to WD formation, yet).

A given starformation history standard model of stellar evolution allows for calculating birth rate of WDs of different masses along the lifetime of the analyzed population. Then, using the standard model of WD cooling, we can obtain the luminosity function and compare it with observational data. If they coincide, then there is no necessity to introduce additional cooling agents. Oppositely, deviations can be attributed, for example, to the effect of axions. Axion cooling can also modify stellar evolution and, thus, indirectly influence WD luminosity function, see, e.g., [137].

The number of known WDs and precision of determination of their parameters rapidly grow in our century thanks to many surveys, especially SDSS and Gaia (see, e.g., [138] and references therein). This allows for determining with high confidence different features, including the change of the slope of the luminosity function due to neutrino cooling in hot WDs and effects of crystallization in old (and cold) sources. However, some uncertainties prevent equally solid conclusion about the role of axions, as it is more subtle.

In the first place, the history of WD formation rate and details of their Galactic distribution are not known well enough. In particular, recent (1–2 Gyrs) bursts of starformation can modify the luminosity function and result in fallacious conclusions about additional cooling agents. This was recently studied in [136].

In their previous studies [139], these authors already came to the conclusion that inclusion of axion cooling helps to improve coincidence between observational data and theoretical luminosity functions for absolute bolometric magnitude $M_{bol} \sim 6$ –12. The same range of M_{bol} , where models without axion cooling slightly overpredict the number of

sources, was also studied in [136]. The new analysis accounting for possible episodes of intensive starformation confirms the older result favoring axions with masses about few meV and (electron) coupling constant $\sim \text{few} \times 10^{-13} \text{ GeV}^{-1}$. Similar behavior of luminosity functions for WDs in the Galactic halo, thin and thick disks provide support for the authors' conclusions, as starformation histories of these three elements of the Galactic structure might not be strongly correlated. Still, uncertainties remain, and new observations are necessary to improve data on the WD luminosity function and new studies of stellar and WD properties would be beneficial too.

As we already mentioned above, axion cooling influences stellar evolution: stars contract due to the additional channel of energy losses from the region of nuclear reactions. Thus, temperature is increased as well as the rate of reactions. The star evolves faster and its helium core grows more massive. On the other hand, at the asymptotic giant branch, the increase of the helium core mass is smaller in the presence of massive axion-like particles. All this results in the mass of a WD, i.e., the relation between initial stellar mass and the compact object mass (IFMR) is modified.

Properties of the IFMR were studied recently in [140]. These authors slightly improve constraints in comparison to those obtained from helium burning (so-called horizontal branch) stars. These objects have dense hot cores, and their lifetime can be estimated from observations. Additional cooling due to axions can significantly modify duration of helium burning in contradiction with observations. This excludes massive axion-like particles in the range $\sim 1\text{--}100 \text{ keV}$ with axion–photon coupling constant $g_{a\gamma\gamma} \gtrsim 10^{-10} \text{ GeV}^{-1}$. In [140], the authors enlarge the forbidden area in the region of so-called cosmological triangle with axion masses about hundreds of keV and coupling constant $\sim 10^{-5} \text{ GeV}^{-1}$ analyzing helium core growth at the asymptotic giant branch stage.

In helium burning shells of asymptotic giant branch stars, the temperature is about 15–20 keV. In these conditions, the Primakoff process and photon–photon interaction can result in production of axion-like particles even if their masses exceed a few tens of keV. Additional cooling leads to faster evolution and more active mixing of matter in outer layers. The latter process results in a smaller amount of helium available for burning in the shell and so the mass of carbon-oxygen core grows slower. Finally, the WD originated from this core is lighter than the one which could be formed in the standard scenario without additional cooling.

In [140], the authors used the IFMR based on 14 double WD wide binary systems. This IFMR covers the range progenitor masses from 2 up to $7M_{\odot}$. If massive ($\sim 10\text{--}100 \text{ keV}$) axion-like particles are considered for $g_{a\gamma\gamma} \gtrsim 10^{-10} \text{ GeV}^{-1}$, theoretical IFMR starts to be outside of the limits defined by observations in the region of progenitor masses $\sim 4\text{--}7 M_{\odot}$ (excluding very large values $g_{a\gamma\gamma} \gtrsim 10^{-3} \text{ GeV}^{-1}$ where other effects become important as axion-like particles do not leave the helium burning shell, but decay inside it). Accounting for rotation slightly softens the constraint, but still it increases the forbidden area in comparison with limits based on analysis of core helium-burning stars.

Maybe the most interesting constraint using WDs is obtained from the analysis of a pulsating source belonging to the so-called ZZ Ceti class (on formation of this type of WDs, see e.g., [141] and references therein). These WDs are situated in the instability strip of the Hertzsprung–Russel diagram. They are middle-aged ($< 10^9 \text{ yrs}$) and thus still warm ($> 10^4 \text{ K}$) objects with convective envelopes containing zones of partial ionization and hydrogen atmospheres.

The constraint is based on observations of pulsation period evolution of G117–B15A—a near ($\approx 57.5 \text{ pc}$) WD with temperature $T \approx 12,000 \text{ K}$ and mass $\sim 0.5 M_{\odot}$. This source has been monitored since the mid-1970s. ZZ Ceti stars increase the pulsation period as they cool down. In the simplest model, $\dot{P}/P \propto -\dot{T}/T$ (e.g., [3]). G117–B15A has a period equal to 215.2 s, and it is increasing with the rate $\dot{P} = 5.47 \pm 0.82 \times 10^{-15} \text{ s s}^{-1}$ [142]; less than 10% of this value can be attributed to the proper motion of the source. Already, in [3], it was proposed that a large value of the period derivative ($\dot{P} = 12 \pm 3.5 \times 10^{-15} \text{ s s}^{-1}$ at

that time) can be explained by additional cooling due to axions. In that paper, the authors obtained the value of axion mass about a few meV.

In the new study [142], the authors estimate axion mass as $m_a \cos^2 \beta = 19.9^{+2.1}_{-3.1}$ meV, where $\cos^2 \beta$ is a free parameter ². This value might be considered as an upper limit as several uncertainties remain.

5. Conclusions

Perspectives for laboratory detection of DM particles and axions in the near future are not very bright. Thus, most probably, astronomical data will not only have a chance to continue producing the best upper limits, but also are the number one candidate to provide direct evidence in favor of the existence of such particles. Various approaches related to different types of sources are used in astroparticle physics. However, continuously NSs and WDs are among the best sites to look for effects linked to new physics.

In the review, we presented several lines of consideration to identify observational tests of the existence of exotic particles predicted by theories. We expect that, in the near future, some of them have chances to provide positive results. To name a few:

- deep surveys can identify dim old sources related to isolated NSs heated by DM particles' annihilation;
- dedicated searches for radio emission related to Primakoff processes can result in its detection;
- finally, detailed studies (including polarization) of surface X-ray and optical emission of cooling NSs can also demonstrate effects related to the existence of axions.

Advances in technology promise persistent progress in the sensitivity of astronomical observations in the next decades. All of this increases the opportunities to discover new particles by astronomical means.

Author Contributions: All authors contributed equally to Sections 1 and 5. Section 2 was mainly written by P.T., Section 3 by M.P. and Section 4 by S.P. All authors have read and agreed to the published version of the manuscript.

Funding: M.P. and S.P. were supported by the Ministry of Science and Higher Education of Russian Federation under the contract 075-15-2020-778 in the framework of the Large Scientific Projects program within the national project "Science".

Data Availability Statement: Observational data used in this paper are quoted from the cited works. Data generated from computations are reported in the body of the paper. Additional data can be made available upon reasonable request.

Acknowledgments: The authors are grateful to Sergey Troitsky and Alexey Zhuravlev for helpful discussions.

Conflicts of Interest: The authors declare no conflict of interest.

Abbreviations

The following abbreviations are used in this manuscript:

ALP	Axion-like particle
BH	black hole
BEC	Bose–Einstein condensate
CP	Charge parity
DFSZ	Dine–Fischler–Srednicki–Zhitnitsky model
DM	Dark matter
EM	Electro-magnetic
FRB	Fast radio burst

IFMR	Initial to final mass ratio
KSVZ	Kim–Shifman–Vainshtein–Zakharov model
MWD	Magnetic white dwarf
NS	Neutron star
NFW	Navarro, Frenk and White model
QCD	Quantum chromodynamics
QED	Quantum electrodynamics
SM	Standard model
SMBH	Supermassive black hole
WD	White dwarf
WIMP	Weakly interacting massive particle
XDINS	X-ray dim isolated neutron stars

Notes

- ¹ If the main charge carriers are not electrons, then the n_e, m_e should be substituted for n_c, m_c .
- ² This model-dependent parameter links electron coupling constant g_{ae} to axion mass m_a in the DFSZ model: $g_{ae} = 2.83 \times 10^{-11} m_a / \cos^2 \beta$ and is usually set equal to unity.

References

- Haensel, P.; Potekhin, A.Y.; Yakovlev, D.G. *Neutron Stars 1 : Equation of State and Structure*; Astrophysics and Space Science Library; Springer: New York, NY, USA, 2007; Volume 326. [[CrossRef](#)]
- Yakovlev, D.G.; Pethick, C.J. Neutron star cooling. *Annu. Rev. Astron. Astrophys.* **2004**, *42*, 169–210. [[CrossRef](#)]
- Isern, J.; Hernanz, M.; Garcia-Berro, E. Axion Cooling of White Dwarfs. *Astrophys. J.* **1992**, *392*, L23. [[CrossRef](#)]
- Sedrakian, A. Axion cooling of neutron stars. *Phys. Rev. D* **2016**, *93*, 065044. [[CrossRef](#)]
- Turolla, R.; Zane, S.; Watts, A.L. Magnetars: The physics behind observations. A review. *Rep. Prog. Phys.* **2015**, *78*, 116901. [[CrossRef](#)]
- Ferrario, L.; de Martino, D.; Gänsicke, B.T. Magnetic White Dwarfs. *Space Sci. Rev.* **2015**, *191*, 111–169. [[CrossRef](#)]
- Raffelt, G.G. *Stars as Laboratories for Fundamental Physics: The Astrophysics of Neutrinos, Axions, and Other Weakly Interacting Particles*; The University of Chicago Press: Chicago, IL, USA; London, UK, 1996.
- Colpi, M.; Shapiro, S.L.; Wasserman, I. Boson stars: Gravitational equilibria of self-interacting scalar fields. *Phys. Rev. Lett.* **1986**, *57*, 2485–2488. [[CrossRef](#)]
- Lee, T.D.; Pang, Y. Fermion soliton stars and black holes. *Phys. Rev. D* **1987**, *35*, 3678–3694. [[CrossRef](#)] [[PubMed](#)]
- Brandt, B.B.; Endrődi, G.; Fraga, E.S.; Hippert, M.; Schaffner-Bielich, J.; Schmalzbauer, S. New class of compact stars: Pion stars. *Phys. Rev. D* **2018**, *98*, 094510. [[CrossRef](#)]
- Brayeur, L.; Tinyakov, P. Enhancement of dark matter capture by neutron stars in binary systems. *Phys. Rev. Lett.* **2012**, *109*, 061301. [[CrossRef](#)] [[PubMed](#)]
- Kouvaris, C. WIMP Annihilation and Cooling of Neutron Stars. *Phys. Rev. D* **2008**, *77*, 023006. [[CrossRef](#)]
- Press, W.H.; Spergel, D.N. Capture by the sun of a galactic population of weakly interacting massive particles. *Astrophys. J.* **1985**, *296*, 679–684. [[CrossRef](#)]
- Gould, A. WIMP Distribution in and Evaporation From the Sun. *Astrophys. J.* **1987**, *321*, 560. [[CrossRef](#)]
- Gould, A. Direct and Indirect Capture of Wimps by the Earth. *Astrophys. J.* **1988**, *328*, 919–939. [[CrossRef](#)]
- Collaboration, X.E.N.O.N.; Aprile, E.; Aalbers, J.; Agostini, F.; Alfonsi, M.; Althueser, L.; Amaro, F.D.; Anthony, M.; Arneodo, F.; Baudis, L.; et al. Dark Matter Search Results from a One Ton-Year Exposure of XENON1T. *Phys. Rev. Lett.* **2018**, *121*, 111302. [[CrossRef](#)]
- Collaboration, X.E.N.O.N.; Aprile, E.; Aalbers, J.; Agostini, F.; Alfonsi, M.; Althueser, L.; Amaro, F.D.; Anthony, M.; Antochi, V.C.; Arneodo, F.; et al. Constraining the spin-dependent WIMP-nucleon cross sections with XENON1T. *Phys. Rev. Lett.* **2019**, *122*, 141301. [[CrossRef](#)]
- Akerib, D.S.; Alsum, S.; Araújo, H.M.; Bai, X.; Bailey, A.J.; Balajthy, J.; Beltrame, P.; Bernard, E.P.; Bernstein, A.; Biesiadzinski, T.P.; et al. Limits on spin-dependent WIMP-nucleon cross section obtained from the complete LUX exposure. *Phys. Rev. Lett.* **2017**, *118*, 251302. [[CrossRef](#)] [[PubMed](#)]
- Xia, J.; Abdukerim, A.; Chen, W.; Chen, X.; Chen, Y.; Cui, X.; Fang, D.; Fu, C.; Giboni, K.; Giuliani, F.; et al. PandaX-II Constraints on Spin-Dependent WIMP-Nucleon Effective Interactions. *Phys. Lett. B* **2019**, *792*, 193–198. [[CrossRef](#)]
- Amole, C.; Ardid, M.; Arnquist, I.J.; Asner, D.M.; Baxter, D.; Behnke, E.; Bressler, M.; Broerman, B.; Cao, G.; Chen, C.J.; et al. Dark Matter Search Results from the Complete Exposure of the PICO-60 C₃F₈ Bubble Chamber. *Phys. Rev. D* **2019**, *100*, 022001. [[CrossRef](#)]
- Acevedo, J.F.; Bramante, J.; Goodman, A.; Kopp, J.; Opferkuch, T. Dark Matter, Destroyer of Worlds: Neutrino, Thermal, and Existential Signatures from Black Holes in the Sun and Earth. *J. Cosmol. Astropart. Phys.* **2021**, *04*, 026. [[CrossRef](#)]

22. Bell, N.F.; Busoni, G.; Robles, S.; Virgato, M. Improved Treatment of Dark Matter Capture in Neutron Stars II: Leptonic Targets. *J. Cosmol. Astropart. Phys.* **2021**, *03*, 086. [[CrossRef](#)]
23. Bell, N.F.; Busoni, G.; Robles, S.; Virgato, M. Improved Treatment of Dark Matter Capture in Neutron Stars. *J. Cosmol. Astropart. Phys.* **2020**, *09*, 028. [[CrossRef](#)]
24. Güver, T.; Erkoca, A.E.; Hall Reno, M.; Sarcevic, I. On the capture of dark matter by neutron stars. *J. Cosmol. Astropart. Phys.* **2014**, *05*, 013. [[CrossRef](#)]
25. Capela, F.; Pshirkov, M.; Tinyakov, P. Constraints on Primordial Black Holes as Dark Matter Candidates from Star Formation. *Phys. Rev. D* **2013**, *87*, 023507. [[CrossRef](#)]
26. Capela, F.; Pshirkov, M.; Tinyakov, P. Adiabatic contraction revisited: Implications for primordial black holes. *Phys. Rev. D* **2014**, *90*, 083507. [[CrossRef](#)]
27. Kouvaris, C.; Tinyakov, P. Constraining Asymmetric Dark Matter through observations of compact stars. *Phys. Rev. D* **2011**, *83*, 083512. [[CrossRef](#)]
28. Goldman, I.; Nussinov, S. Weakly Interacting Massive Particles and Neutron Stars. *Phys. Rev. D* **1989**, *40*, 3221–3230. [[CrossRef](#)]
29. Bertoni, B.; Nelson, A.E.; Reddy, S. Dark Matter Thermalization in Neutron Stars. *Phys. Rev. D* **2013**, *88*, 123505. [[CrossRef](#)]
30. Cermeño, M.; Pérez-García, M.A.; Silk, J. Fermionic Light Dark Matter Particles and the New Physics of Neutron Stars. *Publ. Astron. Soc. Austral.* **2017**, *34*, e043. [[CrossRef](#)]
31. Garani, R.; Genolini, Y.; Hambye, T. New Analysis of Neutron Star Constraints on Asymmetric Dark Matter. *J. Cosmol. Astropart. Phys.* **2019**, *05*, 035. [[CrossRef](#)]
32. Garani, R.; Gupta, A.; Raj, N. Observing the thermalization of dark matter in neutron stars. *Phys. Rev. D* **2021**, *103*, 043019. [[CrossRef](#)]
33. Montero-Camacho, P.; Fang, X.; Vasquez, G.; Silva, M.; Hirata, C.M. Revisiting constraints on asteroid-mass primordial black holes as dark matter candidates. *J. Cosmol. Astropart. Phys.* **2019**, *2019*, 031. [[CrossRef](#)]
34. Kouvaris, C.; Tinyakov, P. Can Neutron stars constrain Dark Matter? *Phys. Rev. D* **2010**, *82*, 063531. [[CrossRef](#)]
35. Leane, R.K.; Linden, T.; Mukhopadhyay, P.; Toro, N. Celestial-Body Focused Dark Matter Annihilation Throughout the Galaxy. *Phys. Rev. D* **2021**, *103*, 075030. [[CrossRef](#)]
36. Garani, R.; Palomares-Ruiz, S. Evaporation of dark matter from celestial bodies. *arXiv* **2021**, arXiv:2104.12757.
37. Baryakhtar, M.; Bramante, J.; Li, S.W.; Linden, T.; Raj, N. Dark Kinetic Heating of Neutron Stars and An Infrared Window On WIMPs, SIMPs, and Pure Higgsinos. *Phys. Rev. Lett.* **2017**, *119*, 131801. [[CrossRef](#)] [[PubMed](#)]
38. Raj, N.; Tanedo, P.; Yu, H.B. Neutron stars at the dark matter direct detection frontier. *Phys. Rev. D* **2018**, *97*, 043006. [[CrossRef](#)]
39. Bell, N.F.; Busoni, G.; Robles, S. Heating up Neutron Stars with Inelastic Dark Matter. *J. Cosmol. Astropart. Phys.* **2018**, *09*, 018. [[CrossRef](#)]
40. Acevedo, J.F.; Bramante, J.; Leane, R.K.; Raj, N. Warming Nuclear Pasta with Dark Matter: Kinetic and Annihilation Heating of Neutron Star Crusts. *J. Cosmol. Astropart. Phys.* **2020**, *03*, 038. [[CrossRef](#)]
41. Joglekar, A.; Raj, N.; Tanedo, P.; Yu, H.B. Dark kinetic heating of neutron stars from contact interactions with relativistic targets. *Phys. Rev. D* **2020**, *102*, 123002. [[CrossRef](#)]
42. Panotopoulos, G.; Lopes, I. Constraints on light dark matter particles using white dwarf stars. *Int. J. Mod. Phys. D* **2020**, *29*, 2050058. [[CrossRef](#)]
43. Cermeño, M.; Pérez-García, M.A. Gamma rays from dark mediators in white dwarfs. *Phys. Rev. D* **2018**, *98*, 063002. [[CrossRef](#)]
44. Gonzalez, D.; Reisenegger, A. Internal Heating of Old Neutron Stars: Contrasting Different Mechanisms. *Astron. Astrophys.* **2010**, *522*, A16. [[CrossRef](#)]
45. Hamaguchi, K.; Nagata, N.; Yanagi, K. Dark Matter Heating vs. Rotochemical Heating in Old Neutron Stars. *Phys. Lett. B* **2019**, *795*, 484–489. [[CrossRef](#)]
46. Casanellas, J.; Lopes, I. Towards the use of asteroseismology to investigate the nature of dark matter. *Mon. Not. R. Astron. Soc.* **2011**, *410*, 535–540. [[CrossRef](#)]
47. Camargo, D.A.; Queiroz, F.S.; Sturani, R. Detecting Dark Matter with Neutron Star Spectroscopy. *J. Cosmol. Astropart. Phys.* **2019**, *09*, 051. [[CrossRef](#)]
48. Graham, P.W.; Rajendran, S.; Varela, J. Dark Matter Triggers of Supernovae. *Phys. Rev. D* **2015**, *92*, 063007. [[CrossRef](#)]
49. Graham, P.W.; Janish, R.; Narayan, V.; Rajendran, S.; Riggins, P. White Dwarfs as Dark Matter Detectors. *Phys. Rev. D* **2018**, *98*, 115027. [[CrossRef](#)]
50. Bell, N.F.; Busoni, G.; Robles, S. Capture of Leptophilic Dark Matter in Neutron Stars. *J. Cosmol. Astropart. Phys.* **2019**, *06*, 054. [[CrossRef](#)]
51. Acevedo, J.F.; Bramante, J. Supernovae Sparked By Dark Matter in White Dwarfs. *Phys. Rev. D* **2019**, *100*, 043020. [[CrossRef](#)]
52. Janish, R.; Narayan, V.; Riggins, P. Type Ia supernovae from dark matter core collapse. *Phys. Rev. D* **2019**, *100*, 035008. [[CrossRef](#)]
53. Petraki, K.; Volkas, R.R. Review of asymmetric dark matter. *Int. J. Mod. Phys. A* **2013**, *28*, 1330028. [[CrossRef](#)]
54. Zurek, K.M. Asymmetric Dark Matter: Theories, Signatures, and Constraints. *Phys. Rept.* **2014**, *537*, 91–121. [[CrossRef](#)]
55. Kouvaris, C. Limits on Self-Interacting Dark Matter. *Phys. Rev. Lett.* **2012**, *108*, 191301. [[CrossRef](#)] [[PubMed](#)]
56. Bramante, J.; Fukushima, K.; Kumar, J.; Stopnitzky, E. Bounds on self-interacting fermion dark matter from observations of old neutron stars. *Phys. Rev. D* **2014**, *89*, 015010. [[CrossRef](#)]
57. Kouvaris, C.; Tinyakov, P.; Tytgat, M.H.G. NonPrimordial Solar Mass Black Holes. *Phys. Rev. Lett.* **2018**, *121*, 221102. [[CrossRef](#)]

58. Gresham, M.I.; Zurek, K.M. Asymmetric Dark Stars and Neutron Star Stability. *Phys. Rev. D* **2019**, *99*, 083008. [[CrossRef](#)]
59. Kouvaris, C.; Tinyakov, P. Excluding Light Asymmetric Bosonic Dark Matter. *Phys. Rev. Lett.* **2011**, *107*, 091301. [[CrossRef](#)] [[PubMed](#)]
60. McDermott, S.D.; Yu, H.B.; Zurek, K.M. Constraints on Scalar Asymmetric Dark Matter from Black Hole Formation in Neutron Stars. *Phys. Rev. D* **2012**, *85*, 023519. [[CrossRef](#)]
61. Kouvaris, C.; Tinyakov, P. (Not)-constraining heavy asymmetric bosonic dark matter. *Phys. Rev. D* **2013**, *87*, 123537. [[CrossRef](#)]
62. Bell, N.F.; Melatos, A.; Petraki, K. Realistic neutron star constraints on bosonic asymmetric dark matter. *Phys. Rev. D* **2013**, *87*, 123507. [[CrossRef](#)]
63. Kurita, Y.; Nakano, H. Gravitational waves from dark matter collapse in a star. *Phys. Rev. D* **2016**, *93*, 023508. [[CrossRef](#)]
64. Bramante, J.; Linden, T.; Tsai, Y.D. Searching for dark matter with neutron star mergers and quiet kilonovae. *Phys. Rev. D* **2018**, *97*, 055016. [[CrossRef](#)]
65. Takhistov, V. Transmuted Gravity Wave Signals from Primordial Black Holes. *Phys. Lett. B* **2018**, *782*, 77–82. [[CrossRef](#)]
66. Nelson, A.; Reddy, S.; Zhou, D. Dark halos around neutron stars and gravitational waves. *J. Cosmol. Astropart. Phys.* **2019**, *07*, 012. [[CrossRef](#)]
67. Bramante, J.; Linden, T. Detecting Dark Matter with Imploding Pulsars in the Galactic Center. *Phys. Rev. Lett.* **2014**, *113*, 191301. [[CrossRef](#)] [[PubMed](#)]
68. Bramante, J.; Elahi, F. Higgs portals to pulsar collapse. *Phys. Rev. D* **2015**, *91*, 115001. [[CrossRef](#)]
69. Bramante, J. Dark matter ignition of type Ia supernovae. *Phys. Rev. Lett.* **2015**, *115*, 141301. [[CrossRef](#)] [[PubMed](#)]
70. Casanellas, J.; Lopes, I. Signatures of dark matter burning in nuclear star clusters. *Astrophys. J. Lett.* **2011**, *733*, L51. [[CrossRef](#)]
71. Abbott, B.P.; Abbott, R.; Abbott, T.D.; Abraham, S.; Acernese, F.; Ackley, K.; Adams, C.; Adhikari, R.X.; Adya, V.B.; Affeldt, C.; et al. Search for Subsolar Mass Ultracompact Binaries in Advanced LIGO's Second Observing Run. *Phys. Rev. Lett.* **2019**, *123*, 161102. [[CrossRef](#)] [[PubMed](#)]
72. Peccei, R.D.; Quinn, H.R. CP conservation in the presence of pseudoparticles. *Phys. Rev. Lett.* **1977**, *38*, 1440–1443. [[CrossRef](#)]
73. Wilczek, F. Problem of strong P and T invariance in the presence of instantons. *Phys. Rev. Lett.* **1978**, *40*, 279–282. [[CrossRef](#)]
74. Weinberg, S. A new light boson? *Phys. Rev. Lett.* **1978**, *40*, 223–226. [[CrossRef](#)]
75. Kim, J.E. Weak-interaction singlet and strong CP invariance. *Phys. Rev. Lett.* **1979**, *43*, 103–107. [[CrossRef](#)]
76. Shifman, M.A.; Vainshtein, A.I.; Zakharov, V.I. Can confinement ensure natural CP invariance of strong interactions? *Nucl. Phys. B* **1980**, *166*, 493–506. [[CrossRef](#)]
77. Zhitnitsky, A.R. On Possible Suppression of the Axion Hadron Interactions. *Sov. J. Nucl. Phys.* **1980**, *31*, 260. (In Russian)
78. Dine, M.; Fischler, W.; Srednicki, M. A simple solution to the strong CP problem with a harmless axion. *Phys. Lett. B* **1981**, *104*, 199–202. [[CrossRef](#)]
79. Svrcek, P.; Witten, E. Axions in string theory. *J. High Energy Phys.* **2006**, *2006*, 051. [[CrossRef](#)]
80. Choi, K.S.; Nilles, H.P.; Ramos-Sánchez, S.; Vaudevange, P.K.S. Accions. *Phys. Lett. B* **2009**, *675*, 381–386. [[CrossRef](#)]
81. Arvanitaki, A.; Dimopoulos, S.; Dubovsky, S.; Kaloper, N.; March-Russell, J. String axiverse. *Phys. Rev. D* **2010**, *81*, 123530. [[CrossRef](#)]
82. Preskill, J.; Wise, M.B.; Wilczek, F. Cosmology of the invisible axion. *Phys. Lett. B* **1983**, *120*, 127–132. [[CrossRef](#)]
83. Abbott, L.F.; Sikivie, P. A cosmological bound on the invisible axion. *Phys. Lett. B* **1983**, *120*, 133–136. [[CrossRef](#)]
84. Particle Data Group; Zyla, P.A.; Barnett, R.M.; Beringer, J.; Dahl, O.; Dwyer, D.A.; Groom, D.E.; Lin, C.J.; Lugovsky, K.S.; Pianori, E.; et al. Review of Particle Physics. *Prog. Theor. Exp. Phys.* **2020**, *2020*, 083C01. [[CrossRef](#)]
85. Wilczek, F. Two Applications of Axion Electrodynamics. *Phys. Rev. Lett.* **1987**, *58*, 1799. [[CrossRef](#)] [[PubMed](#)]
86. Battye, R.A.; Garbrecht, B.; McDonald, J.I.; Pace, F.; Srinivasan, S. Dark matter axion detection in the radio/mm waveband. *Phys. Rev. D* **2020**, *102*, 023504. [[CrossRef](#)]
87. Raffelt, G.; Stodolsky, L. Mixing of the photon with low-mass particles. *Phys. Rev. D* **1988**, *37*, 1237–1249. [[CrossRef](#)]
88. Fairbairn, M.; Rashba, T.; Troitsky, S. Photon-axion mixing and ultra-high energy cosmic rays from BL Lac type objects: Shining light through the Universe. *Phys. Rev. D* **2011**, *84*, 125019. [[CrossRef](#)]
89. Potekhin, A.Y.; Lai, D.; Chabrier, G.; Ho, W.C.G. Electromagnetic Polarization in Partially Ionized Plasmas with Strong Magnetic Fields and Neutron Star Atmosphere Models. *Astrophys. J.* **2004**, *612*, 1034–1043. [[CrossRef](#)]
90. Morris, D.E. Axion mass limits may be improved by pulsar X-ray measurements. *Phys. Rev. D* **1986**, *34*, 843–848. [[CrossRef](#)] [[PubMed](#)]
91. Lai, D.; Heyl, J. Probing axions with radiation from magnetic stars. *Phys. Rev. D* **2006**, *74*, 123003. [[CrossRef](#)]
92. Chelouche, D.; Rabadán, R.; Pavlov, S.S.; Castejón, F. Spectral Signatures of Photon-Particle Oscillations from Celestial Objects. *Astrophys. J. Suppl. Ser.* **2009**, *180*, 1–29. [[CrossRef](#)]
93. Perna, R.; Ho, W.C.G.; Verde, L.; van Adelsberg, M.; Jimenez, R. Signatures of Photon-Axion Conversion in the Thermal Spectra and Polarization of Neutron Stars. *Astrophys. J.* **2012**, *748*, 116. [[CrossRef](#)]
94. Iwamoto, N. Axion Emission From Neutron Stars. *Phys. Rev. Lett.* **1984**, *53*, 1198–1201. [[CrossRef](#)]
95. Nakagawa, M.; Adachi, T.; Kohyama, Y.; Itoh, N. Axion Bremsstrahlung in Dense Stars. II. Phonon Contributions. *Astrophys. J.* **1988**, *326*, 241. [[CrossRef](#)]
96. Fortin, J.F.; Sinha, K. Constraining axion-like-particles with hard X-ray emission from magnetars. *J. High Energy Phys.* **2018**, *2018*, 48. [[CrossRef](#)]

97. Buschmann, M.; Co, R.T.; Dessert, C.; Safdi, B.R. Axion Emission Can Explain a New Hard X-Ray Excess from Nearby Isolated Neutron Stars. *Phys. Rev. Lett.* **2021**, *126*, 021102. [[CrossRef](#)]
98. van Adelsberg, M.; Lai, D. Atmosphere models of magnetized neutron stars: QED effects, radiation spectra and polarization signals. *Mon. Not. R. Astron. Soc.* **2006**, *373*, 1495–1522. [[CrossRef](#)]
99. Fortin, J.F.; Sinha, K. X-ray polarization signals from magnetars with axion-like-particles. *J. High Energy Phys.* **2019**, *2019*, 163. [[CrossRef](#)]
100. Lloyd, S.J.; Chadwick, P.M.; Brown, A.M.; Guo, H.K.; Sinha, K. Axion constraints from quiescent soft gamma-ray emission from magnetars. *Phys. Rev. D* **2021**, *103*, 023010. [[CrossRef](#)]
101. Fortin, J.F.; Guo, H.K.; Harris, S.P.; Sheridan, E.; Sinha, K. Magnetars and axion-like particles: Probes with the hard X-ray spectrum. *J. Cosmol. Astropart. Phys.* **2021**, *2021*, 036. [[CrossRef](#)]
102. Posselt, B.; Popov, S.B.; Haberl, F.; Trümper, J.; Turolla, R.; Neuhäuser, R. The Magnificent Seven in the dusty prairie. *Astrophys. J.* **2007**, *308*, 171–179. [[CrossRef](#)]
103. Dessert, C.; Foster, J.W.; Safdi, B.R. Hard X-ray Excess from the Magnificent Seven Neutron Stars. *Astrophys. J.* **2020**, *904*, 42. [[CrossRef](#)]
104. Zhuravlev, A.; Popov, S.; Pshirkov, M. Photon-axion mixing in thermal emission of isolated neutron stars. *Phys. Lett. B* **2021**, *821*, 136615. [[CrossRef](#)]
105. Barret, D.; Lam Trong, T.; den Herder, J.W.; Piro, L.; Barcons, X.; Huovelin, J.; Kelley, R.; Mas-Hesse, J.M.; Mitsuda, K.; Paltani, S.; et al. The Athena X-ray Integral Field Unit (X-IFU). In Proceedings of the Space Telescopes and Instrumentation 2016: Ultraviolet to Gamma Ray, Edinburgh, UK, 26 June–1 June 2016. [[CrossRef](#)]
106. Soffitta, P.; Barcons, X.; Bellazzini, R.; Braga, J.; Costa, E.; Fraser, G.W.; Gburek, S.; Huovelin, J.; Matt, G.; Pearce, M.; et al. XIPE: The X-ray imaging polarimetry explorer. *Exp. Astron.* **2013**, *36*, 523–567. [[CrossRef](#)]
107. Pshirkov, M.S.; Popov, S.B. Conversion of dark matter axions to photons in magnetospheres of neutron stars. *Sov. J. Exp. Theor. Phys.* **2009**, *108*, 384–388. [[CrossRef](#)]
108. Du, N.; Force, N.; Khatiwada, R.; Lentz, E.; Ottens, R.; Rosenberg, L.J.; Rybka, G.; Carosi, G.; Woollett, N.; Bowring, D.; et al. Search for Invisible Axion Dark Matter with the Axion Dark Matter Experiment. *Phys. Rev. Lett.* **2018**, *120*, 151301. [[CrossRef](#)]
109. Huang, F.P.; Kadota, K.; Sekiguchi, T.; Tashiro, H. Radio telescope search for the resonant conversion of cold dark matter axions from the magnetized astrophysical sources. *Phys. Rev. D* **2018**, *97*, 123001. [[CrossRef](#)]
110. Hook, A.; Kahn, Y.; Safdi, B.R.; Sun, Z. Radio Signals from Axion Dark Matter Conversion in Neutron Star Magnetospheres. *Phys. Rev. Lett.* **2018**, *121*, 241102. [[CrossRef](#)]
111. Safdi, B.R.; Sun, Z.; Chen, A.Y. Detecting axion dark matter with radio lines from neutron star populations. *Phys. Rev. D* **2019**, *99*, 123021. [[CrossRef](#)]
112. Leroy, M.; Chianese, M.; Edwards, T.D.P.; Weniger, C. Radio signal of axion–photon conversion in neutron stars: A ray tracing analysis. *Phys. Rev. D* **2020**, *101*, 123003. [[CrossRef](#)]
113. Witte, S.J.; Noordhuis, D.; Edwards, T.D.P.; Weniger, C. axion–photon Conversion in Neutron Star Magnetospheres: The Role of the Plasma in the Goldreich-Julian Model. *arXiv* **2021**, arXiv:2104.07670.
114. Battye, R.A.; Garbrecht, B.; McDonald, J.; Srinivasan, S. Radio line properties of axion dark matter conversion in neutron stars. *J. High Energy Phys.* **2021**, *2021*, 105. [[CrossRef](#)]
115. Foster, J.W.; Kahn, Y.; Macias, O.; Sun, Z.; Eatough, R.P.; Kondratiev, V.I.; Peters, W.M.; Weniger, C.; Safdi, B.R. Green Bank and Effelsberg Radio Telescope Searches for Axion Dark Matter Conversion in Neutron Star Magnetospheres. *Phys. Rev. Lett.* **2020**, *125*, 171301. [[CrossRef](#)] [[PubMed](#)]
116. Darling, J. Search for Axionic Dark Matter Using the Magnetar PSR J1745-2900. *Phys. Rev. Lett.* **2020**, *125*, 121103. [[CrossRef](#)] [[PubMed](#)]
117. Darling, J. New Limits on Axionic Dark Matter from the Magnetar PSR J1745-2900. *Astrophys. J. Lett.* **2020**, *900*, L28. [[CrossRef](#)]
118. Battye, R.A.; Darling, J.; McDonald, J.; Srinivasan, S. Towards Robust Constraints on Axion Dark Matter using PSR J1745-2900. *arXiv* **2021**, arXiv:2107.01225.
119. Navarro, J.F.; Frenk, C.S.; White, S.D.M. A Universal Density Profile from Hierarchical Clustering. *Astrophys. J.* **1997**, *490*, 493–508. [[CrossRef](#)]
120. Wang, J.W.; Bi, X.J.; Yao, R.M.; Yin, P.F. Exploring axion dark matter through radio signals from magnetic white dwarf stars. *Phys. Rev. D* **2021**, *103*, 115021. [[CrossRef](#)]
121. Lorimer, D.R.; Bailes, M.; McLaughlin, M.A.; Narkevic, D.J.; Crawford, F. A Bright Millisecond Radio Burst of Extragalactic Origin. *Science* **2007**, *318*, 777. [[CrossRef](#)]
122. Popov, S.B.; Postnov, K.A.; Pshirkov, M.S. Fast radio bursts. *Phys. Uspekhi* **2018**, *61*, 965. [[CrossRef](#)]
123. Zhang, B. The physical mechanisms of fast radio bursts. *Nature* **2020**, *587*, 45–53. [[CrossRef](#)]
124. Xiao, D.; Wang, F.; Dai, Z. The physics of fast radio bursts. *Sci. China Phys. Mech. Astron.* **2021**, *64*, 249501. [[CrossRef](#)]
125. Tkachev, I.I. Fast radio bursts and axion miniclusters. *Sov. J. Exp. Theor. Phys. Lett.* **2015**, *101*, 1–6. [[CrossRef](#)]
126. Iwazaki, A. Axion stars and fast radio bursts. *Phys. Rev. D* **2015**, *91*, 023008. [[CrossRef](#)]
127. Pshirkov, M.S. May axion clusters be sources of fast radio bursts? *Int. J. Mod. Phys. D* **2017**, *26*, 1750068. [[CrossRef](#)]
128. Prabhu, A.; Rapidis, N.M. Resonant conversion of dark matter oscillons in pulsar magnetospheres. *J. Cosmol. Astropart. Phys.* **2020**, *2020*, 054. [[CrossRef](#)]

129. Buckley, J.H.; Dev, P.S.B.; Ferrer, F.; Huang, F.P. Fast radio bursts from axion stars moving through pulsar magnetospheres. *Phys. Rev. D* **2021**, *103*, 043015. [[CrossRef](#)]
130. Raffelt, G.G. Axion constraints from white dwarf cooling times. *Phys. Lett. B* **1986**, *166*, 402–406. [[CrossRef](#)]
131. Dessert, C.; Long, A.J.; Safdi, B.R. X-ray Signatures of Axion Conversion in Magnetic White Dwarf Stars. *Phys. Rev. Lett.* **2019**, *123*, 061104. [[CrossRef](#)]
132. Ferrario, L.; Wickramasinghe, D.; Kawka, A. Magnetic fields in isolated and interacting white dwarfs. *Adv. Space Res.* **2020**, *66*, 1025–1056. [[CrossRef](#)]
133. Dessert, C.; Long, A.J.; Safdi, B.R. No evidence for axions from Chandra observation of magnetic white dwarf. *arXiv* **2021**, arXiv:2104.12772.
134. Anastassopoulos, V.; Aune, S.; Barth, K.; Belov, A.; Bräuninger, H.; Cantatore, G.; Carmona, J.M.; Castel, J.F.; Cetin, S.A.; Christensen, F.; et al. New CAST limit on the axion–photon interaction. *Nat. Phys.* **2017**, *13*, 584–590. [[CrossRef](#)]
135. Gill, R.; Heyl, J.S. Constraining the photon-axion coupling constant with magnetic white dwarfs. *Phys. Rev. D* **2011**, *84*, 085001. [[CrossRef](#)]
136. Isern, J.; García-Berro, E.; Torres, S.; Cojocaru, R.; Catalán, S. Axions and the luminosity function of white dwarfs: The thin and thick discs, and the halo. *Mon. Not. R. Astron. Soc.* **2018**, *478*, 2569–2575. [[CrossRef](#)]
137. Raffelt, G.G. Astrophysical Axion Bounds. In *Axions*; Kuster, M., Raffelt, G., Beltrán, B., Eds.; Springer: Berlin/Heidelberg, Germany, 2008; Volume 741, p. 51.
138. Gentile Fusillo, N.P.; Tremblay, P.E.; Gänsicke, B.T.; Manser, C.J.; Cunningham, T.; Cukanovaite, E.; Hollands, M.; Marsh, T.; Raddi, R.; Jordan, S.; et al. A Gaia Data Release 2 catalogue of white dwarfs and a comparison with SDSS. *Mon. Not. R. Astron. Soc.* **2019**, *482*, 4570–4591. [[CrossRef](#)]
139. Isern, J.; García-Berro, E.; Torres, S.; Catalán, S. Axions and the Cooling of White Dwarf Stars. *Astrophys. J. Lett.* **2008**, *682*, L109. [[CrossRef](#)]
140. Dolan, M.J.; Hiskens, F.J.; Volkas, R.R. Constraining axion-like particles using the white dwarf initial-final mass relation. *J. Cosmol. Astropart. Phys.* **2021**, *2021*, 010. [[CrossRef](#)]
141. Althaus, L.G.; Serenelli, A.M.; Córscico, A.H.; Benvenuto, O.G. Evolution of a $3-M_{\text{solar}}$ star from the main sequence to the ZZ Ceti stage: The role played by element diffusion. *Mon. Not. R. Astron. Soc.* **2002**, *330*, 685–698. [[CrossRef](#)]
142. Kepler, S.O.; Winget, D.E.; Vanderbosch, Z.P.; Castanheira, B.G.; Hermes, J.J.; Bell, K.J.; Mullally, F.; Romero, A.D.; Montgomery, M.H.; DeGennaro, S.; et al. The Pulsating White Dwarf G117-B15A: Still the Most Stable Optical Clock Known. *Astrophys. J.* **2021**, *906*, 7. [[CrossRef](#)]